nature communications

Article

https://doi.org/10.1038/s41467-024-50782-3

A conserved oomycete effector RxLR23 triggers plant defense responses by targeting ERD15La to release NbNAC68

Received: 20 May 2023

Accepted: 19 July 2024

Published online: 27 July 2024

Check for updates

Hui Sheng[1], Congcong Ai[1], Cancan Yang[1], Chunyuan Zhu[2], Zhe Meng[3], Fengzhi Wu[4], Xiaodan Wang[5], Daolong Dou[6], Paul F. Morris[7] & Xiuguo Zhang[1]

Oomycete pathogens deliver many effectors to enhance virulence or suppress plant immunity. Plant immune networks are interconnected, in which a few effectors can trigger a strong defense response when recognized by immunity-related proteins. How effectors activate plant defense response remains poorly understood. Here we report *Phytophthora capsici* effector RxLR23^{KM} can induce plant cell death and plant immunity. RxLR23^{KM} specifically binds to ERD15La, a regulator of abscisic acid and salicylic acid pathway, and the binding intensity depends on the amino acid residues (K^{93} and M^{320}). NbNAC68, a downstream protein of ERD15La, can stimulate plant immunity that is compromised after binding with ERD15La. Silencing of NbNAC68 substantially prevents the activation of plant defense response. RxLR23^{KM} binds to ERD15La, releasing NbNAC68 to activate plant immunity. These findings highlight a strategy of plant defense response that ERD15La as a central regulator coordinates RxLR23^{KM} to regulate NbNAC68-triggered plant immunity.

Plants have evolved sophisticated defense systems that are deployed against insects, bacteria, fungi, oomycete, and virus[1–3]. Conceptionally, these systems have been recently described as three-layered defense network[1], consisting of a recognition layer, an internal layer that integrates both apoplastic and internal cellular signals, and a defense response layer. Apoplastic signaling can be triggered by Pathogen/Microbe Associated Molecular Patterns (PAMPs/MAMPs) or Damage Associated Molecular Patterns (DAMPs), leading to PTI[4–8]. Functionally, these defense systems are highly buffered. At the recognition layer, receptors contribute to activating multiple genes in the signaling layer. When the pattern-triggered signaling in the signal integration layer is interfered by effectors, which inhibits the receptor to trigger an immune response, resulting in the activation of other genes[9]. From the pathogen's perspective, it is likely that there is no single strategy that will enable it to be successful.

Oomycete pathogens are easily to hazard a wide range of plant species. Oomycete pathogen genomes encode a large number of proteins that can promote infection or trigger plant immunity. For instance, *Phytophthora* pathogens secrete cytoplasmic effectors, mainly containing RxLR and CRN families, to target various compartments or pathways in their hosts[10,11]. To date, more than 37 oomycete species have accomplished genome sequencing, in which a large number of effectors was predicted[12]. RxLR effectors, existing more than one hundred in each *Phytophthora* genome, are the best-characterized oomycete effectors[13–16]. The *P. capsici* secretome includes at least 640 RxLR and 59 CRN predicted effectors that are delivered into the host cytoplasm[17–19]. RxLR effectors were named by their conserved Arg-any amino acid Leu-Arg (RxLR) motif at the N-terminus[15,16]. RxLR motif carried out to facilitate delivery and translocation of effectors to host cells[20,21]. Accumulating evidence

[1]Shandong Provincial Key Laboratory for Biology of Vegetable Diseases and Insect Pests, College of Plant Protection, Shandong Agricultural University, Tai'an 271018, China. [2]State Key Laboratory of Crop Biology, College of Life Sciences, Shandong Agricultural University, Tai'an 271018, China. [3]College of Life Sciences, Shandong Normal University, Ji'nan 250014, China. [4]Department of Horticulture, Northeast Agricultural University, Harbin 150030, China. [5]College of Plant Protection, China Agricultural University, 100083 Beijing, China. [6]Department of Plant Pathology, Nanjing Agricultural University, Nanjing 210095, China. [7]Department of Biological Sciences, Bowling Green State University, Bowling Green, OH 43043, USA. e-mail: zhxg@sdau.edu.cn

demonstrates that some RxLR effectors utilize various mechanisms to promote infection[22–24], while some RxLR effectors act on manipulating various aspects of plant defence[25]. Significantly, some of the characterized RxLR effectors inhibit signaling pathways activated by the recognition layer. Members of these effectors targeted proteins that are components of the signal integration layer[26–32], and others inhibit defense responses such as RNAi, ROS and programmed cell death[33–38]. Several effectors have been confirmed to inhibit salicylic acid (SA) pathway[39–42]. The disruption of this pathway achieved by diversion of precursors metabolites, inhibition of the genes required for SA synthesis, promotion of the breakdown of SA pathway, and interference with downstream SA signaling[39,43,44]. In recent years, abundant evidences have elucidated the biological functions of some RxLR effectors from *P. infestans*, *P. sojae* and *Hyaloperonospora arabidopsidis*[22,25,45–47]. However, little is known about RxLR effectors functions from *P. capsici*.

The transcription factor EARLY RESPONSIVE TO DEHYDRATION 15 (ERD15) was first identified as a dehydration-induced gene from *Arabidopsis thaliana*[48,49]. Expression of ERD15 is elevated in response to various abiotic and biotic stresses[50] and has been demonstrated to function as a common regulator of Abscisic Acid (ABA) response and SA-dependent defense pathway[51]. Notably, ERD15 proteins from different plant species operate in cross-talk among different response pathways[50]. For example, a soybean ERD15 homolog can trigger NRP protein-mediated cell death in response to osmotic and endoplasmic reticulum stresses[49]. Significantly, ERD15 can influence plant-pathogen interactions[51], and modulate multi-defense genes expression mediated by abiotic and biotic stress signals[51,52], thereby activating plant resistance. Taken together, these data indicate that ERD15 acts as both a negative regulator of ABA signaling and a promoter of PR pathway responses[50]. Until now, this protein has not been identified as a target of effectors related to plant defense responses.

NAC (NAM, ATAF and CUC) protein member is one of the largest plant-specific transcription factors (TFs) families. NAC proteins play varied roles in plant diverse biological processes[53–55], and perform critical roles in biotic and abiotic stress signaling[56–58]. Numerous NAC genes are involved in reducing or enhancing resistance to plant pathogens upon regulating the expression of downstream genes, and integrating hormone and other signals. For example, a few NAC members s from *Oryza sativa* and *Solanum lycopersicum* negatively regulate hosts' resistance to virus[59,60]. *Triticum aestivum* TaNAC1 enhances *Pseudomonas* infection in *Arabidopsis*[61], while StNACb4 and StNAC43 (St: *Solanum tuberosum*) promote resistance to *Ralstonia solanacearum* that is correlated with SA, ABA and MeJA signaling[62]. Many *Oryza sativa* NAC TFs positively regulate rice resistance to blast fungus *Magnaporthe oryzae* via activating SA and MeJA[63], suppressing ABA signaling[64], promoting programmed cell death, accumulating ROS and up-regulating defense-related genes[65]. Both TaNAC2 and TaNAC30 promote *Puccinia* stripe rust (*Pst*) infection by reducing H_2O_2 burst[66,67], while four other TaNAC TFs are involved in defense response to three important fungal diseases[68–70]. Conspicuously, a few oomycete RxLR effectors promote virulence or trigger plant immunity mediated by NAC. For instance, four *Bremia lactucae* RxLR effectors interact with *Lactuca sativa* NAC069 to inhibit its re-localization from endoplasmic reticulum (ER) to nucleus, leading to hindering plant immunity[71]; two *Arabidopsis* NAC TFs, ANAC013 and ANAC017, interact directly with RCD1 that is then targeted by *Hyaloperonospora arabidopsidis* effector HaRxL106, resulting in suppression of plant immunity[44,72]; *P. infestans* RxLR Pi03192 promotes virulence by interacting with two potato membrane-associated NAC TFs followed by preventing re-localization from ER to nucleus[73]. Until now, the mechanisms of NAC TFs involved in pathogen infection or plant defense response is poorly understood. Importantly, RxLR effectors activate NAC TFs to motivate plant immunity mediated by ERD15 that has not been reported.

Phytophthora capsici was first described as filamentous oomycete pathogen in 1996[74]. *P. capsici* is a globally important pathogenic oomycete, capable of infecting plants more than 15 families, and is a threat to many crop species. Here, we identified a crucial effector RxLR23 from *P. capsici*. Our experiments demonstrate that RxLR23 is required for *P. capsici* virulence. However, expression of RxLR23 in *N. benthamiana* triggers plant cell death, ROS accumulation and activation of SA response genes, resulting in inhibition of *P. capsici* infection. $RxLR23^{KM}$ directly and specifically interacts with ERD15La. The characteristics of this effector are correlated to its binding with ERD15La, which is largely due to the amino acid residues of K^{93}(Lys) and M^{320} (Met) in RxLR23 sequence. We further confirmed that NbERD15La negatively regulated $RxLR23^{KM}$-triggered plant immunity, along with increased ABA and reduced SA levels after co-expression of $RxLR23^{KM}$ and NbERD15La in *N. benthamiana*. Furthermore, NbERD15La binds to NbNAC68 and it blocks NbNAC68-activated plant immunity by inhibiting NbNAC68 binding to and activation of *PR1/2* promoters. In addition, NbNAC68 is required for $RxLR23^{KM}$ induced cell death and plant immunity, but the cell death caused by $RxLR23^{KM}$ need to be further investigated. In absence of $RxLR23^{KM}$, the increased expression of NbERD15La enables it to strongly bind with NbNAC68, resulting in blocked defense response. Otherwise, sufficient quantities of $RxLR23^{KM}$ blocks the combination of NbERD15La with NbNAC68, resulting in activation of plant defense response. To summarize, we report $RxLR23^{KM}$ promotes a crucial plant defense system in which sustained interaction of $RxLR23^{KM}$ with NbERD15La triggers activity of NbNAC68 to irritate plant defense response. Significantly, these findings highlight the importance of sustained expression of effectors as a strategy to activate plant immune responses.

Results

RxLR23 is required for full virulence of *P. capsici*

RxLR23 (MT070866.1) was isolated from a virulent *P. capsici* strain SD33[75]. This effector has a requisite signal peptide in the N-terminal sequence with a calculated molecular mass of 40.37 kDa. The RxLR23 sequence in SD33 strain is identical to that in LT1534 (KAG1696733.1) except for the $Y^{5}C$ mutation. To determine the expression patterns of *RxLR23*, we examined this effector expression by qRT-PCR in mycelia, zoospores, germinating cysts, sporangia, and at multiple time points following inoculation zoospores in *Capsicum annuum* inbred line 06221 leaves (Supplementary Fig. 1). The expression levels of *RxLR23* were barely detected in any of the four developmental stages before infection. However, following zoospores inoculation of *C. annuum* leaves, expression levels were 20-fold above background at 0.5 hpi, and by 1.5 hpi were more than 200-fold higher than at 0.5 hpi. Thereafter, expression levels fell sharply by 3 hpi and at times up to 48 hpi were only 25% of 0.5 hpi and then become barely detectable at 72 hpi. This expression pattern indicates that *RxLR23* is expressed only at the very earliest stage of infection, similar to that of *PcAvh1*[76] and *PsCRN108*[77]. For some RxLR effectors, the timing of their expression is critical to their effectiveness as virulent factors[46]. We therefore hypothesized that continued elevated expression of this effector might be detrimental to virulence.

To evaluate the contribution of RxLR23 to the virulence of *P. capsici*, CRISPR/Cas9 was used to generate *RxLR23* knockout mutants[78]. Two mutants T-7 and T-10 were successfully obtained upon replacement of the coding region with *mRFP* gene (Supplementary Fig. 2A, C). An additional mutant T-13 was also recovered with the coding region of *RxLR23* unchanged. Both T-13 and WT (SD33) were used as controls. Sequence analysis of PCR fragments determined the loss of the gene (Supplementary Fig. 2B). PCR amplification confirmed that T-7 and T-10 were homozygous knockouts (Supplementary Fig. 2C). Southern blot analysis of *Hind*III digested genomic DNA using an mRFP probe identified a single band (2818 bp) in two transformed

https://doi.org/10.1038/s41467-024-50782-3

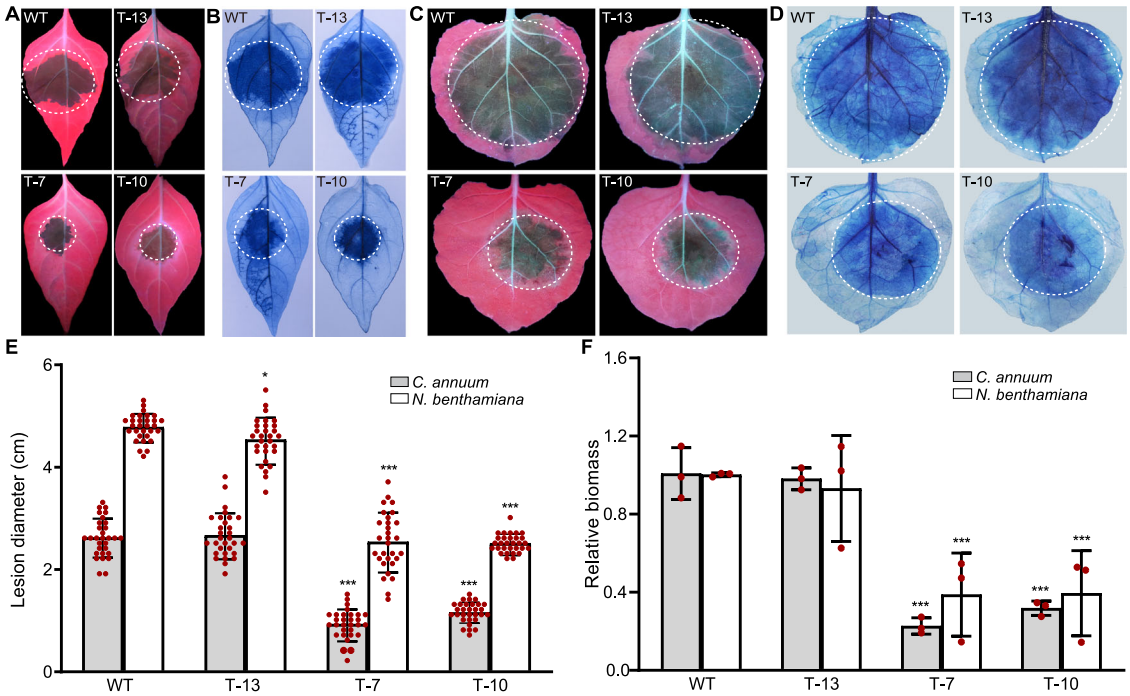

Fig. 1 | RxLR23 effector is required for virulence of *P. capsici*. **A**, **C** Virulence of *RxLR23* knockout mutants acts on *C. annuum* and *N. benthamiana* leaves. T-7 and T-10 are knockout mutants. T-13 is an unknockout mutant. WT is SD33 strain. Leaves of *C. annuum* and *N. benthamiana* were inoculated with *P. capsici* zoospores from T-7, T-10, T-13, or WT strain. Images were taken under UV light for *C. annuum* leaves at 72 hpi and for *N. benthamiana* leaves at 48 hpi ($n = 30$ samples). **B**, **D** Cell death was scored by trypan blue staining on *C. annuum* and *N. benthamiana* leaves, respectively ($n = 30$ samples). **E** Lesion spread diameter of 30 leaves infected by mutants relative to WT in *C. annuum* or *N. benthamiana* leaves. Values are presented as mean ± SD, $n = 30$ samples (ANOVA, $^{*}p < 0.05$, $^{***}p < 0.001$). **F** qPCR was used to measure the relative biomass on the ratios of *P. capsici* to *C. annuum* or *N. benthamiana* DNA at 48 hpi. *Pcβ-actin*, *CaEIF5A2*, and *NbEF1α* were identified as the most suitable reference genes for normalization. The degree of relative biomass of infected *C. annuum* or *N. benthamiana* leaves with WT strain was assigned to value 1.0. The data graphs present the means and error bars represent ± S.D from three independent experiments (ANOVA, $^{***}p < 0.001$). These experiments (**A**–**E**) were repeated at least three times. Source data are provided as a Source Data file.

lines (Supplementary Fig. 2C). The T-7 and T-10 did not alter mycelial growth rate, colonial characteristics, sporangial morphology and size, and number of releasing zoospores compared with WT and T-13 strains (Supplementary Fig. 2D–H).

To determine whether the loss of RxLR23 affected *P. capsici* virulence, zoospores of the two edited T-7 and T-10, the unedited T-13, and WT strains were prepared and used to inoculate *C. annuum* and *N. benthamiana* leaves. Virulence of T-13 was almost equal to WT. However, both T-7 and T-10 produced small lesions on *C. annuum* leaves (approximately 35% of control strains) and *N. benthamiana* leaves (approximately 50% of control strains) (Fig. 1A, C, E). Trypan blue staining further confirmed that cell death of leaves caused by the knockout lines in *C. annuum* and *N. benthamiana* leaves was restricted to the significantly small area surrounding the inoculation sites in contrast to control strains (Fig. 1B, D). To assess the infection more precisely, qPCR was used to measure the relative *P. capsici* biomass (the ratio of *P. capsici* DNA to *C. annuum* and *N. benthamiana* DNA) in infected tissues (Fig. 1F). These data indicated that the loss of this effector reduced the growth rate of *P. capsici* in *C. annuum* and *N. benthamiana* to one-third to a half of the rate of the control strains. In summary, the deletion of this effector significantly reduced the virulence of *P. capsici* in both *C. annuum* and *N. benthamiana* and RxLR23 is required for maximum virulence during *P. capsici* infection.

RxLR23 induces cell death that is associated with two critical amino acid residues of its sequence

To elucidate whether RxLR23 could cause cell death in plant tissues, *Agrobacterium* strains expressing pBinGFP2:RxLR23, pBinGFP2:INF1, and pBinGFP2 were infiltrated into *N. benthamiana* leaves alone. pBinGFP2:INF1 was used as the positive control[79]. pBinGFP2 was used as the negative control. Infiltration of RxLR23 induced cell death, but it was not as intense as INF1. Significantly, RxLR23 was strongly expressed in both cytoplasm and nucleus and with additional expression in the nucleolus in contrast to GFP (Supplementary Fig. 3D). To determine whether the cell death caused by RxLR23 was related to the subcellular localization, pBinGFP2:RxLR23, pBinGFP2:$_{NLS}$RxLR23, and pBinGFP2:$_{NES}$RxLR23 were ectopically expressed in *N. benthamiana* leaves, respectively. $_{NES}$RxLR23 excluded the fluorescence from the nucleolus, while $_{NLS}$RxLR23 restricted the fluorescence to the nucleus (Supplementary Fig. 3D). In contrast to RxLR23, cell death caused by $_{NES}$RxLR23 was obviously reduced, whereas cell death was only slightly reduced after expression of $_{NLS}$RxLR23 (Supplementary Fig. 3A, B). $_{NLS}$RxLR23 elicited a stronger cell death response than $_{NES}$RxLR23. This result is associated with the percentage of electrolyte leakage in infiltrated sites (Supplementary Fig. 3C). The leaf samples were obtained after expression of each construct at 48 h, and then western blot confirmed that the expected protein size of each construct was present in the leaf extracts (Supplementary Fig. 3E). Localization to the nucleus region of the core effector Pi04314 was also correlated with the virulence of *P. infestans*[80]. In our study, cell necrosis induced by RxLR23 was stronger related to localization of this effector to nucleus than to cytoplasm. Plant hypersensitive response (HR) is characterized by rapid cell death at the inoculation sites and is associated with disease resistance. In our study, RxLR23 induced plant cell death at 4 dpi, suggesting this may be hypersensitive-like cell death. In summary, RxLR23 caused cell death response that is related to its localization to both cytoplasm and nucleus, but RxLR23 elicited a stronger cell death response in nucleus than in cytoplasm.

https://doi.org/10.1038/s41467-024-50782-3

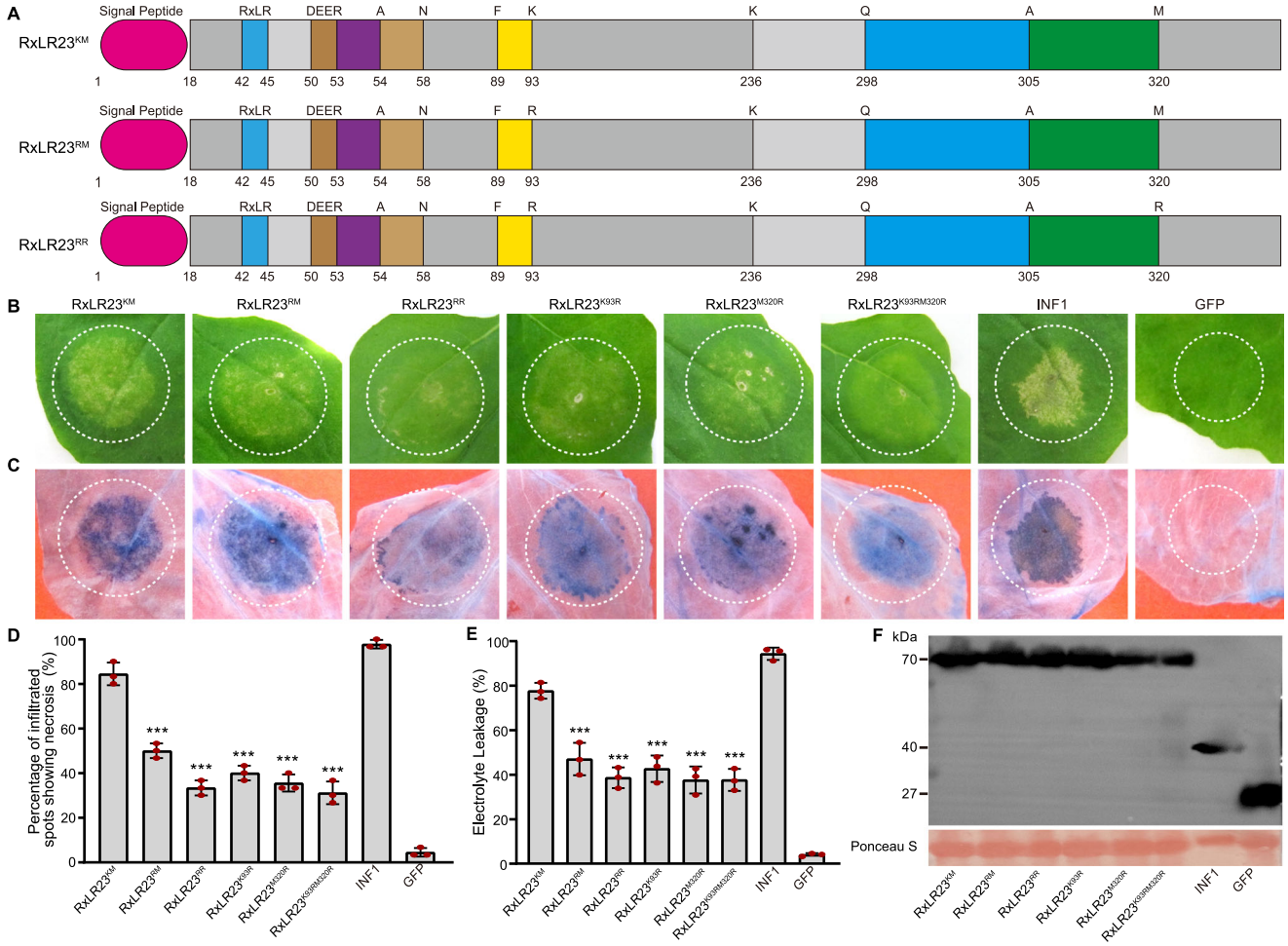

Fig. 2 | RxLR23^{KM} and its five allelic variants arouse various degrees of cell death responses in *N. benthamiana*. **A** The mutations of two key amino acids (K^{93}: Lysine and M^{320}: Methionine) in RxLR23 sequence from different virulence *P. capsici* strains. The RxLR23 sequence shows that these two key amino acids are K^{93} and M^{320} (named as RxLR23^{KM}) in a highly virulent strain SD33. RxLR23 sequence contains an allelic variant of K^{93}R (named as RxLR23^{RM}) in the mildly virulent strain YN07. The mutations of RxLR23 sequence result in two allelic variants of K^{93}R and M^{320}R (named as RxLR23^{RR}) in the weakly virulent strain Aug0202. Allelic variants of K^{93}R, M^{320}R, and K^{93}RM^{320}R were generated using Fast Site Mutagenesis Kit. **B** Typical lesions caused by ectopic expression of pBinGFP2:RxLR23^{KM} or five allelic variants in *N. benthamiana* at 4 dpi ($n = 30$ samples). **C** Trypan blue staining of agroinfiltration sites highlighted cell death by RxLR23^{KM} and its five isoforms at 4 dpi ($n = 30$ samples). **D** Quantification of cell death induced by RxLR23^{KM} and its five isoforms. Percentage of cell death in spots was analyzed from at least 30 leaves. Values are presented as mean ± SD, $n = 3$ independent experiments (ANOVA, $^{***}p < 0.001$). **E** Electrolyte leakage was measured upon expression of RxLR23^{KM} and its five isoforms compared with INF1. Values are presented as mean ± SD, $n = 3$ independent experiments (ANOVA, $^{***}p < 0.001$). **F** Immunoblot analysis of transiently expressed proteins in *N. benthamiana* leaves using anti-GFP antibodies alone. Protein loading is indicated by Ponceau staining (Ponceau S). These experiments (**B**, **C**, **F**) were repeated at least three times. Source data are provided as a Source Data file.

In prior work, we characterized three *P. capsici* strains (SD33, YN07, and Aug0202) that showed different virulence (Supplementary Table 1). Sequence alignment of allelic variants of this effector from these three strains revealed that only two amino acids were changed (Fig. 2A and Supplementary Fig. 4). In the highly virulent strain SD33, RxLR23 sequence, emerging two amino acids K^{93} and M^{320}, was named RxLR23^{KM}. In the mildly virulent strain YN07, RxLR23 has noted a K^{93}R mutation that was named as RxLR23^{RM}, while RxLR23 was mutated at K^{93}R and M^{320}R in the weakly virulent strain Aug0202 and was named as RxLR23^{RR}. To evaluate whether these two amino acids related to the cell death response, *Agrobacterium* strains carrying pBinGFP2:RxLR23^{KM}, pBinGFP2:RxLR23^{RM}, pBinGFP2:RxLR23^{RR}, pBinGFP2:INF1, and pBinGFP2 (Supplementary Table 3) were infiltrated into *N. benthamiana* leaves alone. pBinGFP2:INF1, and pBinGFP2 were used as positive and negative controls respectively. Virulence was assessed by analysis of necrosis and trypan blue staining after 4 dpi. RxLR23^{KM} triggered obvious cell death responses in the leaves, while five allelic variants showed reduced levels of necrotic lesions relative to RxLR23^{KM}. This data was quantified by measuring the percentage of infiltrated regions with necrotic spots and the percentage of electrolyte leakage from infiltrated regions (Fig. 2B–E). In each case, western blot detection of protein extracts from the inoculation spots confirmed that these constructs were expressed as intact proteins in *N. benthamiana* (Fig. 2F). To investigate whether cell death response caused by RxLR23^{KM} and its five allelic variations related to their subcellular localizations, six GFP-fusion constructs were expressed in *N. benthamiana* leaves and their localizations were observed by confocal microscopy. As a result, RxLR23^{KM} and its five alleles showed similar cytoplasm/nuclear/nucleolar localization (Supplementary Fig. 5). Thus, variation of cell death response caused by RxLR23^{KM} and its five alleles is not correlated with their subcellular localization. In summary, RxLR23 induces cell death that is associated with two critical amino acid residues of its sequence.

RxLR23 triggers plant immune against *P. capsici* infection

Since RxLR23 was required for full virulence of *P. capsici* and triggered cell death at 4 d after infiltration (Figs. 1 and 2), we hypothesized that ectopic expression of this effector might trigger plant immune response before it caused cell death. To test this

https://doi.org/10.1038/s41467-024-50782-3

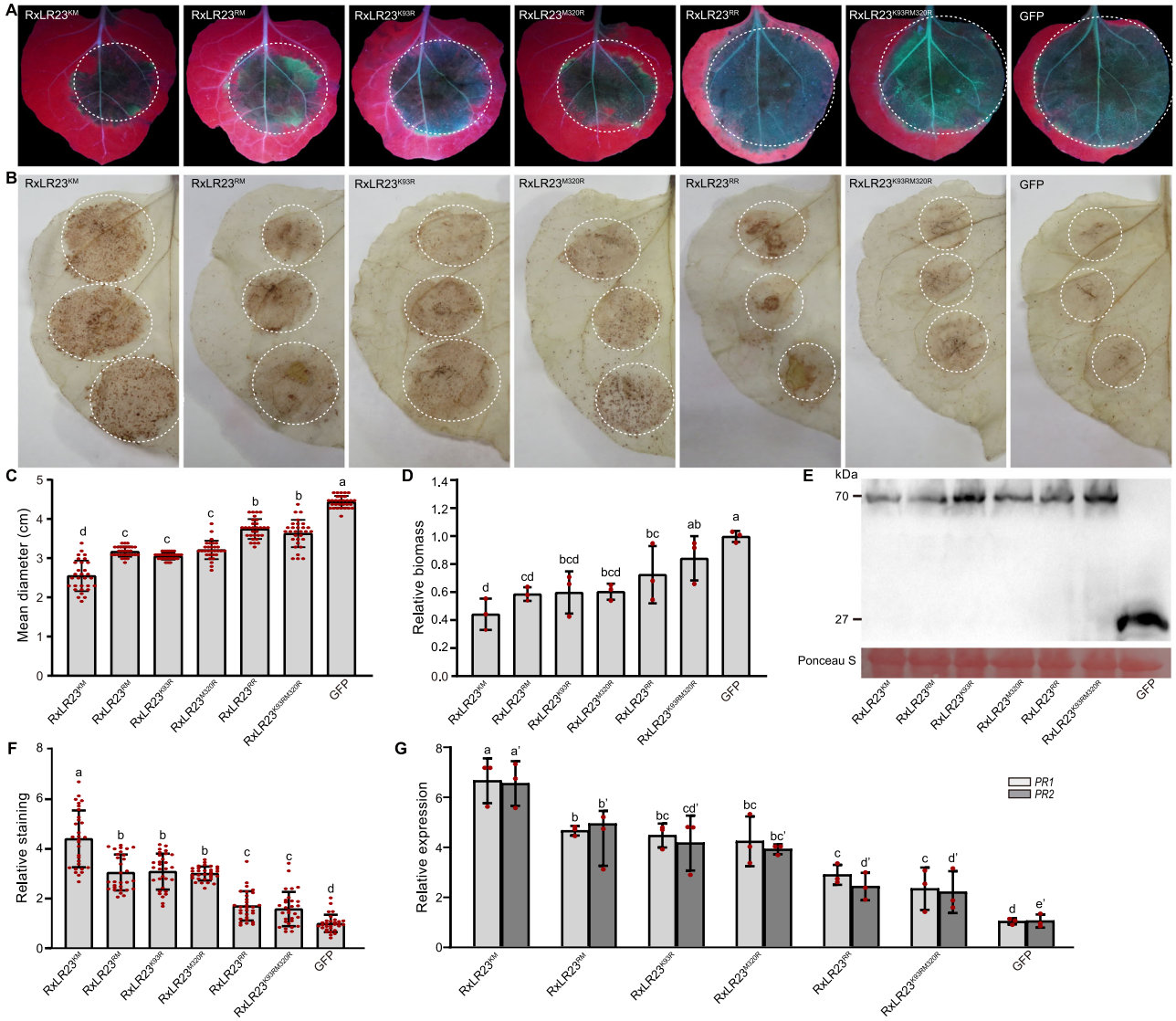

Fig. 3 | Expression of RxLR23^{KM} and its five allelic variants trigger various levels of plant defense against *P. capsici* infection. A pBinGFP2:RxLR23^{KM}, pBinGFP2:RxLR23^{RM}, pBinGFP2:RxLR23^{RR}, pBinGFP2:RxLR23^{K93R}, pBinGFP2:RxLR23^{M320R}, pBinGFP2:RxLR23^{K93RM320R}, or pBinGFP2 was transiently expressed in *N. benthamiana* leaves and subsequently inoculated with *P. capsici* zoospores at 24 h ($n = 30$ samples). Representative lesions were taken under UV irradiation at 48 hpi. **B** H_2O_2 accumulation in *N. benthamiana* leaves was examined by DAB staining after inoculation with each construct at 36 h ($n = 30$ samples). **C** Mean diameter of lesions was measured in *N. benthamiana* leaves after inoculation with *P. capsici* at 48 h. Values are presented as mean ± SD, $n = 30$ samples. **D** qPCR was used to measure the relative biomass on the ratios of *P. capsici* to *N. benthamiana* leaves DNA after inoculation with *P. capsici* at 48 h. *Pcβ-actin* and *NbEF1α* were identified as the most suitable reference genes for normalization. The ratio expressing GFP was assigned to value 1.0. Values are presented as mean ± SD, $n = 3$ independent experiments. **E** Expected protein sizes of RxLR23^{KM} and its five isoforms were detected by western blots using GFP-antibodies alone. Protein loading is indicated by Ponceau staining (Ponceau S). **F** Relative levels of DAB staining were examined after inoculation at 36 h. The relative staining of GFP was assigned to value 1.0. Values are presented as mean ± SD, $n = 30$ samples. **G** Relative expression levels of *PR1/2* were detected in *N. benthamiana* leaves after expression of each construct at 48 h. *NbEF1α* of *N. benthamiana* was as constitutively expressed endogenous control. Values are presented as mean ± SD, $n = 3$ independent experiments. The data in (**C**, **D**, **F**, **G**) were analyzed by ANOVA one-way comparison followed by least significant difference (LSD) test and different letters above the bars indicate a significant difference at $p < 0.05$. These experiments (**A**–**C**, **E**, **F**) were repeated at least three times. Source data are provided as a Source Data file.

hypothesis, *N. benthamiana* leaves were infiltrated with RxLR23^{KM} or five allelic variants and subsequently inoculated with *P. capsici* zoospores at 24 h. Expression of RxLR23^{KM} resulted in a significant reduction of lesion size relative to GFP at 48 hpi (Fig. 3A, C). This inhibition was also correlated with lower levels of pathogen biomass (Fig. 3D). In contrast to GFP, prior expression of five allelic variants of RxLR23^{KM} also resulted in a subsequent inhibition of *P. capsici* infection, but they were less potent than RxLR23^{KM} (Fig. 3A, C, D). Expected protein sizes of RxLR23^{KM} and its five alleles in leaf extracts were verified by western blots (Fig. 3E). DAB staining of the leaf tissues showed that the inhibition of infection was directly correlated with a strong ROS response at the point of inoculation (Fig. 3B, F). Transient expression of RxLR23^{KM} in *N. benthamiana* leaves produced the most potent ROS response in contrast to its allelic variants. To further confirm that RxLR23^{KM} triggered immune response, we also monitored the expression of the resistance-related genes *PR1/2*. Expression of RxLR23^{KM} resulted in a stronger expression level of *PR1/2* compared with its five allelic variants (Fig. 3G). Therefore, the amino acid residues K^{93} and M^{320} play a crucial role in triggering plant immune against *P. capsici* infection.

To further evaluate the effect of RxLR23^{KM}, RxLR23^{RM}, and RxLR23^{RR} on plant resistance, five transgenic lines of RxLR23^{KM} or RxLR23^{RM}, and four transgenic lines of RxLR23^{RR} were obtained from the second generation of transgenic plants. T1 and T3 lines of RxLR23^{KM}, T7 and T10 lines of RxLR23^{RM}, and T11 and T13 lines of RxLR23^{RR} were used to observe their response to *P. capsici* infection, respectively. Seedlings of these six lines are visibly stunted, and the leaf size is smaller by 50% ~ 60% than CK and WT plants (Supplementary Fig. 6A–D). Expression of RxLR23^{KM}, RxLR23^{RM}, RxLR23^{RR}, and GFP in the respective lines was confirmed by western blot (Supplementary Fig. 6E).

To investigate whether all these transgenic lines could inhibit *P. capsici* infection, we inoculated each transgenic line with *P. capsici* zoospores. In contrast to CK and WT, the lesion diameter was reduced by two-thirds in transgenic leaves of RxLR23^{KM}, and the lesion diameter was reduced by one-third in transgenic leaves of RxLR23^{RM} (Supplementary Fig. 7A, B). However, the lesion diameter in RxLR23^{RR} transgenic leaves is slightly smaller than that of CK and WT leaves. All these results are supported by the various trends of *P. capsici* biomass and the expression patterns of *PR1/2* (Supplementary Fig. 7C, D). Thus, ectopic expression of RxLR23 in *Arabidopsis* can enhance disease resistance, especially, these two residues (K^{93} and M^{320}) involve in RxLR23 inducing plant immunity. In summary, RxLR23 is required for maximum virulence at the early stages of *P. capsici* infection, but continuous expression of this effector results in the activation of defense responses that include the upregulation of *PR1/2*.

Interaction of RxLR23^{KM} with ERD15La

To identify possible host targets of RxLR23^{KM}, a yeast library of 2×10^7 clones from *C. annuum* leaves infection with *P. capsici* was screened using pGBKT7:RxLR23^{KM} as the bait. One candidate protein (XP_016543747.2) was recovered several times, with homology to Early Responsive to Dehydration Like (ERD15L) from *A. thaliana*. This sequence was named CaERD15La (Supplementary Table 4). Two related sequences in the *C. annuum* genome were named as CaERD15Lb (XP_016571847.1) and CaERD15Lc (XP_016558122.1), respectively. CaERD15Lb and CaERD15Lc shares 75% and 55% identity with CaERD15La alone, but CaERD15Lb is 67% identical to CaERD15Lc. We BLAST-searched CaERD15La amino acid sequence in the *N. benthamiana* genome. Three orthologous ERD15L proteins were identified in *N. benthamiana* genome, named as NbERD15La (Niben101Scf04038g03011.1), NbERD15Lb (Niben101Scf04411g02006.1), and NbERD15Lc (Niben 101Scf01578g00008.1), respectively (Supplementary Table 4). NbERD15La is 84% identical to CaERD15La, while NbERD15Lb/c shares 81% and 80% identity with CaERD15La alone (Supplementary Fig. 8A and Supplementary Table 4). Notably, NtERD15 shares 95% identity with NbERD15Lc, CaERD15La is 96.15% identical toSlERD15L. Each sequence of ERD15L and ERD15 contains highly conserved PAM2 and PAE1 domains in N-terminal and a more diverse C-terminal region[48,81,82] (Supplementary Fig. 8A and Supplementary Table 4). Phylogenetically, all these analyzed sequences are grouped into four clusters that are highlighted with different background colors (Supplementary Fig. 8B), suggesting that ERD15L and ERD15 sequences are widely distributed across multiple plant species.

To validate the interaction between RxLR23^{KM} and CaERD15Ls, we performed Y2H and Co-IP assays. RxLR23^{KM} interacted with CaERD15La but not with CaERD15Lb/c (Supplementary Fig. 9A, B). The conserved domain PAM2 in the N-terminal of ERD15L enables ERD15L to directly interact with PABP (PolyA-Binding Proteins)[83,84]. To test whether RxLR23^{KM} interacted with CaERD15La via CaPABP, CaPABP was used as prey in Y2H and fused with FLAG for Co-IP. RxLR23^{KM} did not interact with CaPABP upon both Y2H and Co-IP assays (Supplementary Fig. 9A, B). Thus, CaPABP was not involved in the interaction between RxLR23^{KM} and CaERD15La.

Next, we test whether RxLR23^{KM} interacts with NbERD15Ls. First, Y2H was conducted using RxLR23^{KM} as bait, and the full-length of NbERD15La as prey. The interaction of the two proteins is supported by yeast growth on media lacking adenine and histidine, and the induction of X-α-galactosidase activity (Fig. 4A). To confirm this interaction also occurs *in planta*, Co-IP and BiFC were carried out in *N. benthamiana* leaves alone. NbERD15La was immunoprecipitated by RxLR23^{KM} (Fig. 4B) and the combination of RxLR23^{KM}-YFPn with NbERD15La-YFPc produced a yellow fluorescent in the cytoplasm and nucleus (Fig. 4F). However, Co-IP and BiFC assays did not show an interaction of RxLR23^{KM} with NbERD15Lb/c (Fig. 4C, F). To summarize, these experiments indicate RxLR23^{KM} specifically binds to NbERD15La in both the cytosol and nucleus. Since the amino acid sequences in the C-terminal of ERD15La differ markedly from both ERD15Lb and ERD15Lc (Supplementary Fig. 8A), it is likely that RxLR23^{KM} interacts with the C-terminal of ERD15La in vitro and in vivo. Y2H, Co-IP, and BiFC further confirmed NbERD15La interacted with RxLR23^{KM} in vivo and in vitro, but not with RxLR23^{RM} or RxLR23^{RR} (Fig. 4D–F). Thus, K^{93} and M^{320} are the key amino acid residues for RxLR23^{KM} interaction with NbERD15La, resulting in RxLR23^{KM} triggering stronger cell death and plant defense responses than RxLR23^{RM} or RxLR23^{RR}.

To further determine if RxLR23^{KM} alter the localization of ERD15La, we observe the co-localization of RxLR23^{KM}-GFP with NbERD15La/b/c-RFP by ectopic co-expression in *N. benthamiana* leaves. Confocal images revealed that RxLR23^{KM}-GFP localized to the cytoplasm and nucleus, while NbERD15La/b/c-RFP localized in the cytoplasm and nucleoplasm excluded from the nucleolus. Interestingly, RxLR23^{KM}-GFP with NbERD15La/b/c-RFP is co-localized to the cytoplasm and nucleoplasm (Supplementary Fig. 10A, B). In cells where both fluorescent proteins were expressed, we measured the fluorescence intensity of GFP and RFP along a transect bisecting the nucleus. Fluorescence intensity of RxLR23^{KM}-GFP peaked at the nucleolus, while that of NbERD15La/b/c-RFP dipped, indicating no accumulation in the nucleolus of NbERD15La/b/c in the presence of RxLR23^{KM} (Supplementary Fig. 10C). These fluorescent patterns showed that RxLR23^{KM} did not result in the re-localization of NbERD15La, suggesting that RxLR23^{KM} co-localization with NbERD15La in the cytoplasm and nucleoplasm. To further investigate where RxLR23^{KM} binding to NbERD15La, we detected interaction of RxLR23^{KM}, $_{NES}$RxLR23^{KM} or $_{NLS}$RxLR23^{KM} with NbERD15La using Y2H and LCI assays. The results showed that the interactions of NbERD15La with $_{NES}$RxLR23^{KM} or $_{NLS}$RxLR23^{KM} were weaken relative to RxLR23^{KM} by Y2H and LCI assays (Supplementary Fig. 11A, B). All these results indicate that the functions of RxLR23^{KM} mainly dependent on its specifically interacts with NbERD15La in the cytoplasm and nucleoplasm.

NbERD15La negatively regulated RxLR23^{KM}-triggered plant immunity

Since NbERD15La is a target protein of RxLR23^{KM}, we examined the expression patterns of *NbERD15La/b/c* in *N. benthamiana* leaves following inoculation with *P. capsici* zoospores at multiple time points by qRT-PCR, respectively (Supplementary Fig. 12A). In contrast to 0 hpi, expression of *NbERD15La* occurs in all treated time points after *P. capsici* infection, but it showed strong expression levels from 1.5 to 12 hpi with a spike at 3 hpi. However, NbERD15Lb/c is hardly expressed at multiple time points relative to 0 hpi. Thus, *NbERD15La* is typically activated at early stages of infection, but notably this spike of *NbERD15La* expression occurs later than the peak expression of RxLR23 (Supplementary Fig. 1). To investigate the characteristics of NbERD15La/b/c in plant defense response, NbERD15La/b/c was first transiently expressed in *N. benthamiana* leaves alone and subsequently inoculated with *P. capsici* zoospores. Expression of NbERD15La/b/c did not affect lesion development relative to GFP control (Supplementary Fig. 12B, C). Thus, overexpression of NbERD15La/b/c does not contribute to plant defense response. Next, we used VIGS to knock down

https://doi.org/10.1038/s41467-024-50782-3

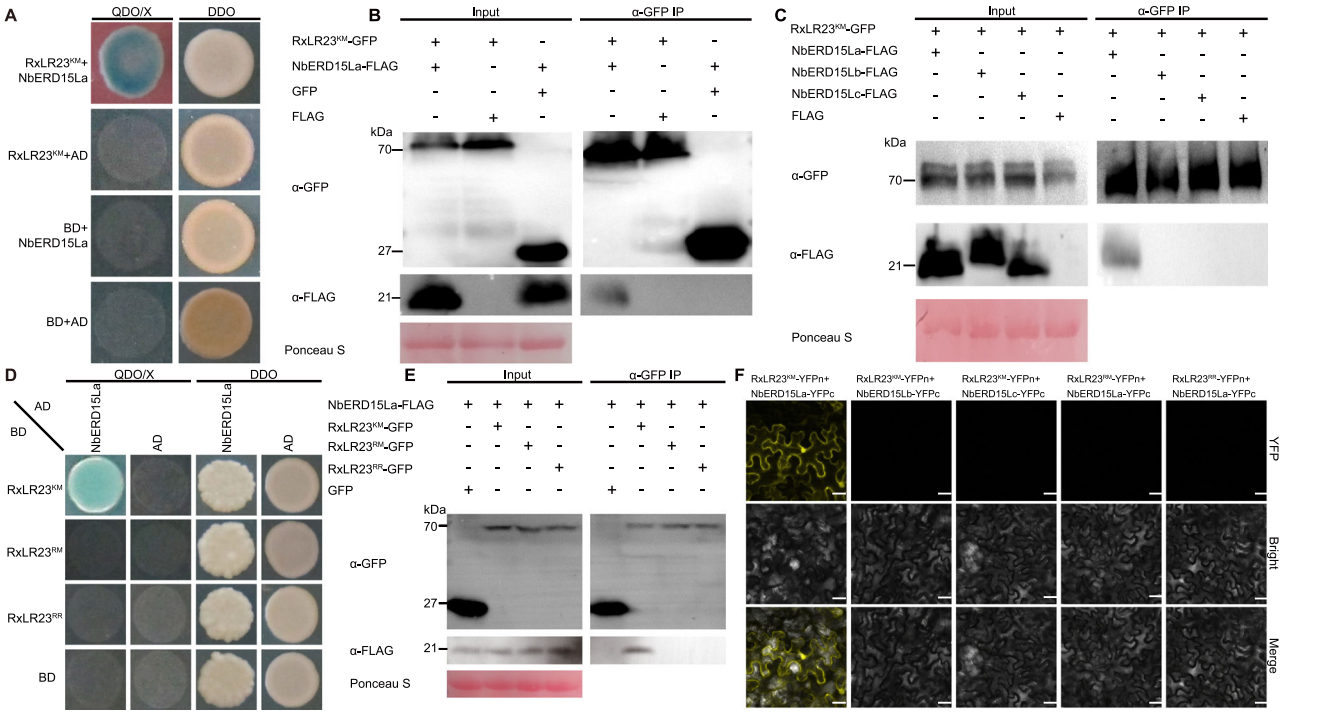

Fig. 4 | RxLR23^{KM} specifically interacts with NbERD15La. A Y2H confirmed that RxLR23^{KM} interacted with NbERD15La in yeast. Yeast transformants were first grown on SD/-Trp/-Leu (DDO), and then selected on SD/-Trp/-Leu/-His/-Ade/X-α-gal (QDO/X) for activating X-α-galactosidase activity. The images were photographed at 4 days after incubation. **B** Co-IP was used to examine the interaction of RxLR23^{KM} with NbERD15La in *N. benthamiana* leaves. Left panels confirm transient expression (+) RxLR23^{KM}-GFP and NbERD15La-FLAG. Equal protein loading is indicated by Ponceau staining (Ponceau S). Right panels show that RxLR23^{KM}-GFP is specifically combined with NbERD15La-FLAG. **C** RxLR23^{KM} uniquely interacts with NbERD15La upon Co-IP assay. Left panels confirmed transient expression (+) RxLR23^{KM}-GFP and NbERD15La/b/c-FLAG. Equal protein loading was indicated by Ponceau staining (Ponceau S). Right panels showed that RxLR23^{KM}-GFP was specifically combined with NbERD15La-FLAG. **D** NbERD15La specifically interacts with RxLR23^{KM} but not with its two allelic variants by Y2H. The images were photographed at 4 days after incubation. **E** The interaction of NbERD15La-FLAG with RxLR23^{KM}-GFP and its two allelic variants was detected using Co-IP in *N. benthamiana* leaves, respectively. Left panels confirmed transient expression of (+) RxLR23^{KM}-GFP, two allelic variants, and NbERD15La-FLAG alone. Equal protein loading was indicated by Ponceau staining (Ponceau S). Right panels showed that NbERD15La-FLAG was specifically combined with RxLR23^{KM}-GFP. **F** BiFC showed RxLR23^{KM} specifically interacted with NbERD15La in the nucleus and cytoplasm. Different pairs of constructs were co-expressed in *N. benthamiana*. The fluorescence was observed and imaged by confocal microscopy at 48 hpi. Scale bars, 20 μm. Each experiment was repeated at least three times. Source data are provided as a Source Data file.

NbERD15La/b/c in *N. benthamiana* alone. In contrast to TRV:GFP, transcription levels of *NbERD15La/b/c* were respectively reduced by 70% to 80% in corresponding to silenced lines (Supplementary Fig. 12D). TRV:NbERD15La/b/c plants exhibit a slightly stunted phenotype compared with TRV:GFP plants, and the newly emerging leaves of TRV:PDS plants were obviously bleached in color (Supplementary Fig. 12E). To evaluate the effect of silencing *NbERD15La/b/c*, TRV:NbERD15La/b/c and TRV:GFP plants were inoculated with *P. capsici* zoospores alone. The lesion diameter and pathogen biomass were significantly reduced in TRV:NbERD15La leaves that is opposed to in TRV:NbERD15Lb or TRV:NbERD15Lc leaves relative to in TRV:GFP leaves (Supplementary Fig. 12F, G), suggesting that NbERD15La was acting as a negative regulator of plant resistance to *P. capsici* infection.

We next investigated whether ERD15La was involved in mediating RxLR23^{KM} to induce cell death. *Agrobacterium* strains harboring pBinGFP2:RxLR23^{KM}, pBinGFP2:INF1, and pBinGFP2 were infiltrated into TRV:NbERD15La/b/c and TRV:GFP leaves, respectively. The cell death response of RxLR23^{KM} was present in TRV:NbERD15La/b/c plants, but the intensity of cell death was directly proportional to the OD *Agrobacterium* cells transfected into the leaf for RxLR23^{KM} expression (Supplementary Fig. 13A, B), which was correlated with the percentage of electrolyte leakage relative to INF1 (Supplementary Fig. 13C). The correct size of each protein was confirmed by western blots (Supplementary Fig. 13D). Thus, the intensity of cell death caused by RxLR23^{KM} is independent of NbERD15La/b/c, but is correlated with the effect of OD on RxLR23^{KM} expression.

In addition, we addressed whether silencing *NbERD15La* affected the plant immune response when ectopic expression of RxLR23^{KM} or GFP in *N. benthamiana* leaves preceded inoculation with *P. capsici* zoospores. In silenced leaves, ectopic expression of GFP resulted in significant smaller lesions than in non-silenced leaves (Fig. 5A, C) and this finding was correlated with less relative biomass and increased DAB staining (Fig. 5B, E). Expression of RxLR23^{KM} in TRV:NbERD15La leaves resulted in smaller lesion diameters (Fig. 5A, C), a greater intensity of DAB staining (Fig. 5B, E), and less pathogen biomass (Fig. 5D). In TRV:NbERD15La or TRV:GFP leaves, co-expression of NbERD15La and RxLR23^{KM} resulted in larger lesion size compared with expressing RxLR23^{KM} respectively (Fig. 5A, C). The lesion size in TRV:NbERD15La leaves is much smaller than in TRV:GFP after expressing GFP (Fig. 5A, C). These results were also supported by the data of *P. capsici* biomass and DAB staining (Fig. 5B, D, E). In addition, the lesion size in TRV:NbERD15La leaves is almost the same as in TRV:GFP leaves after expressing NbERD15La (Fig. 5A, C), which was also associated with the data of *P. capsici* biomass and DAB staining (Fig. 5B, D, E). Expression of all these proteins in silenced and non-silenced leaves was verified by western blot using GFP-antibodies (Fig. 5F). Finally, the changes in all these experiments were correlated with the expression patterns of *PR1/2* in silenced and non-silenced leaves (Fig. 5G). Furthermore, the expression levels of *PR1/2* were upregulated in silenced plants and these patterns were then inhibited in silenced plants after over-expression of NbERD15La. Thus, decreased expression of

https://doi.org/10.1038/s41467-024-50782-3

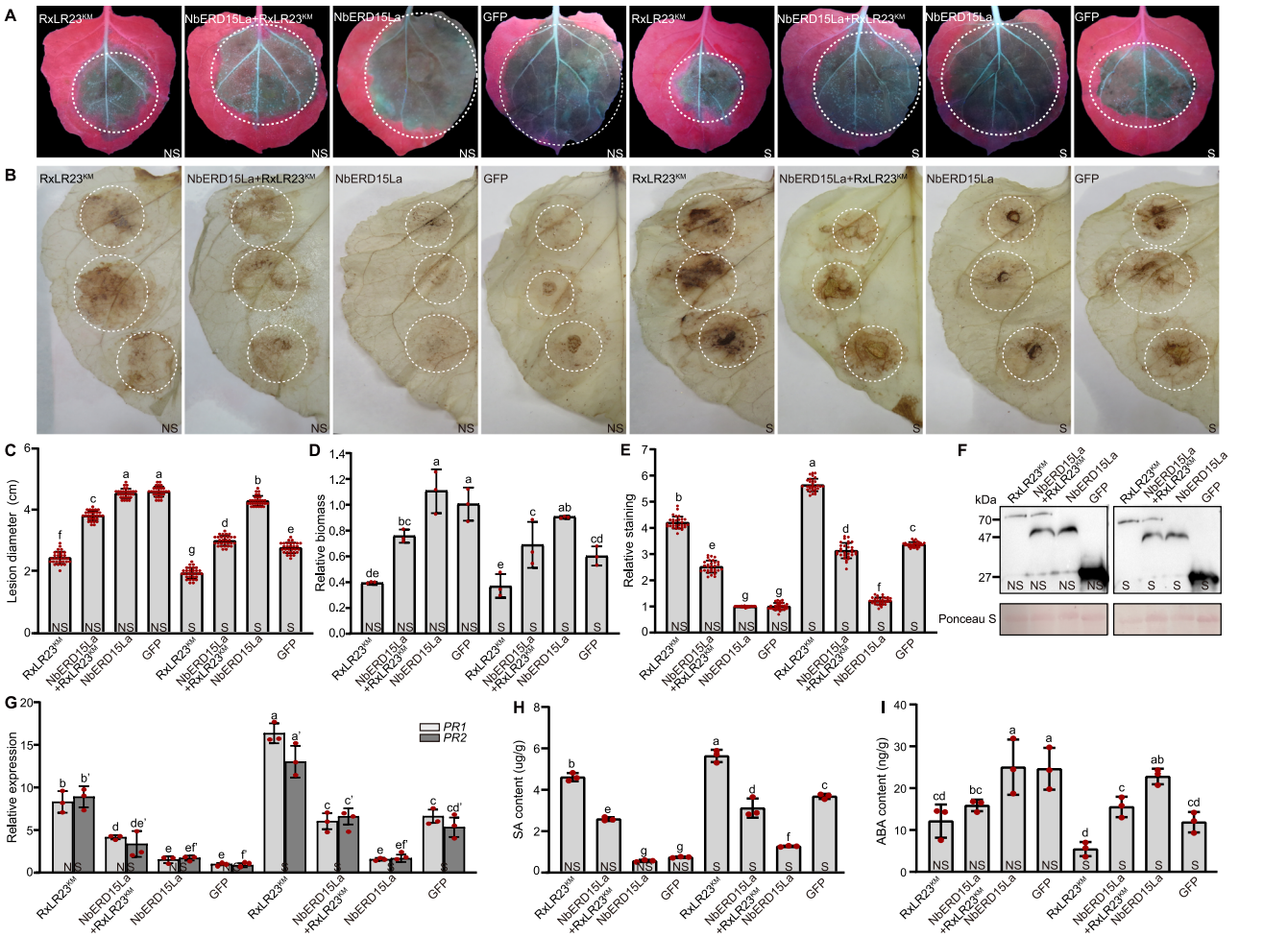

Fig. 5 | NbERD15La negatively regulated RxLR23^{KM}-triggered plant immunity. pBinGFP2:RxLR23^{KM}, pBinGFP2:NbERD15La, NbERD15La + RxLR23^{KM}, and pBinGFP2 were transiently expressed in S (TRV:NbERD15La) and NS (TRV:GFP) *N. benthamiana* leaves alone. The leaves were inoculated with *P. capsici* zoospores after expression of all these constructs at 24 h. **A** Typical lesion images of leaves were photographed under UV irradiation at 48 hpi ($n = 30$ samples). **B** H_2O_2 accumulation in *N. benthamiana* leaves was measured by DAB staining at 36 h ($n = 30$ samples). **C** Mean diameter of lesions was measured at 48 hpi. Values are presented as mean ± SD, $n = 30$ samples. **D** Relative biomass of *P. capsici* was measured by qPCR at 48 hpi. *Pcβ-actin* and *NbEF1α* were identified as the most suitable reference genes for normalization. The ratio in the leaves inoculated with GFP was assigned to value of 1.0. Values are presented as mean ± SD, $n = 3$ independent experiments. **E** Relative levels of DAB staining were examined at 36 h. The relative staining of GFP was assigned to value 1.0. Values are presented as mean ± SD, $n = 3$ independent experiments. **F** Expected proteins size was detected by western blots using GFP-antibodies alone. Protein loading is indicated by Ponceau staining (Ponceau S). **G** Expression levels of both *PR1/2* were detected by qRT-PCR at 48 hpi. *NbEF1α* of *N. benthamiana* was used as constitutively expressed endogenous control. Values are presented as mean ± SD, $n = 3$ independent experiments. **H, I** The variations of SA or ABA content were examined by HPLC-MS in *N. benthamiana* leaves after expressing each of these constructs at 24 h, respectively. Values are presented as mean ± SD, $n = 3$ independent experiments. The data in (**C**–**E**, **G**–**I**) were analyzed by ANOVA one-way comparison followed by least significant difference (LSD) test and different letters above the bars indicate a significant difference at $p < 0.05$. These experiments (**A**–**C**, **E**, **F**) were repeated three times with similar results. Source data are provided as a Source Data file.

NbERD15La resulted in activation of plant immunity and inhibition of *P. capsici* infection.

The plant hormones Salicylic acid (SA) and Abscisic acid (ABA) act as a positive and a negative[49,85,86] regulator of plant immunity, respectively. To further illuminate whether plant defense mediated by RxLR23^{KM} and NbERD15La is related to SA and ABA levels, we measured SA and ABA production in TRV:NbERD15La and TRV:GFP plants after expression of RxLR23^{KM}, RxLR23^{KM} combination with NbERD15La, and NbERD15La at 24 h, respectively. RxLR23^{KM} combination with NbERD15La produced lower SA content and higher ABA content than RxLR23^{KM} in silenced and unsilenced plants alone. In addition, strong increase of SA and decrease of ABA were produced in silenced plants compared with in unsilenced plant after expression of RxLR23^{KM} or GFP, or co-expression of RxLR23^{KM} and NbERD15La (Fig. 5H, I). Thus, RxLR23^{KM} induced increased SA and reduced ABA in plants, which is disturbed by ERD15La, suggesting that ERD15La negatively regulated RxLR23^{KM} triggered SA and ABA pathway. Together, all these results indicated that NbERD15La negatively regulated plant immunity triggered by RxLR23^{KM}.

SA enhanced RxLR23^{KM}-triggered plant defense response by suppressing ERD15La activity

The previous experiments confirmed that SA production in *N. benthamiana* was inhibited by ERD15La expression. To further address whether SA affect the activity of ERD15La, we measured the expression levels of *NbERD15La* by qRT-PCR and quantitative western blot in *N. benthamiana* at multiple time points after treatment with SA or PAC. As previously reported[50], the expression levels of *NbERD15La* were reduced slightly after spraying with SA (Fig. 6A, B). At the same time, spraying leaves with PAC (a potential inhibitor of SA biosynthesis)[87] resulted in a slight decline of SA levels (Supplementary Fig. 14) and a two-fold increase in expression levels of *NbERD15La* (Fig. 6A, B).

https://doi.org/10.1038/s41467-024-50782-3

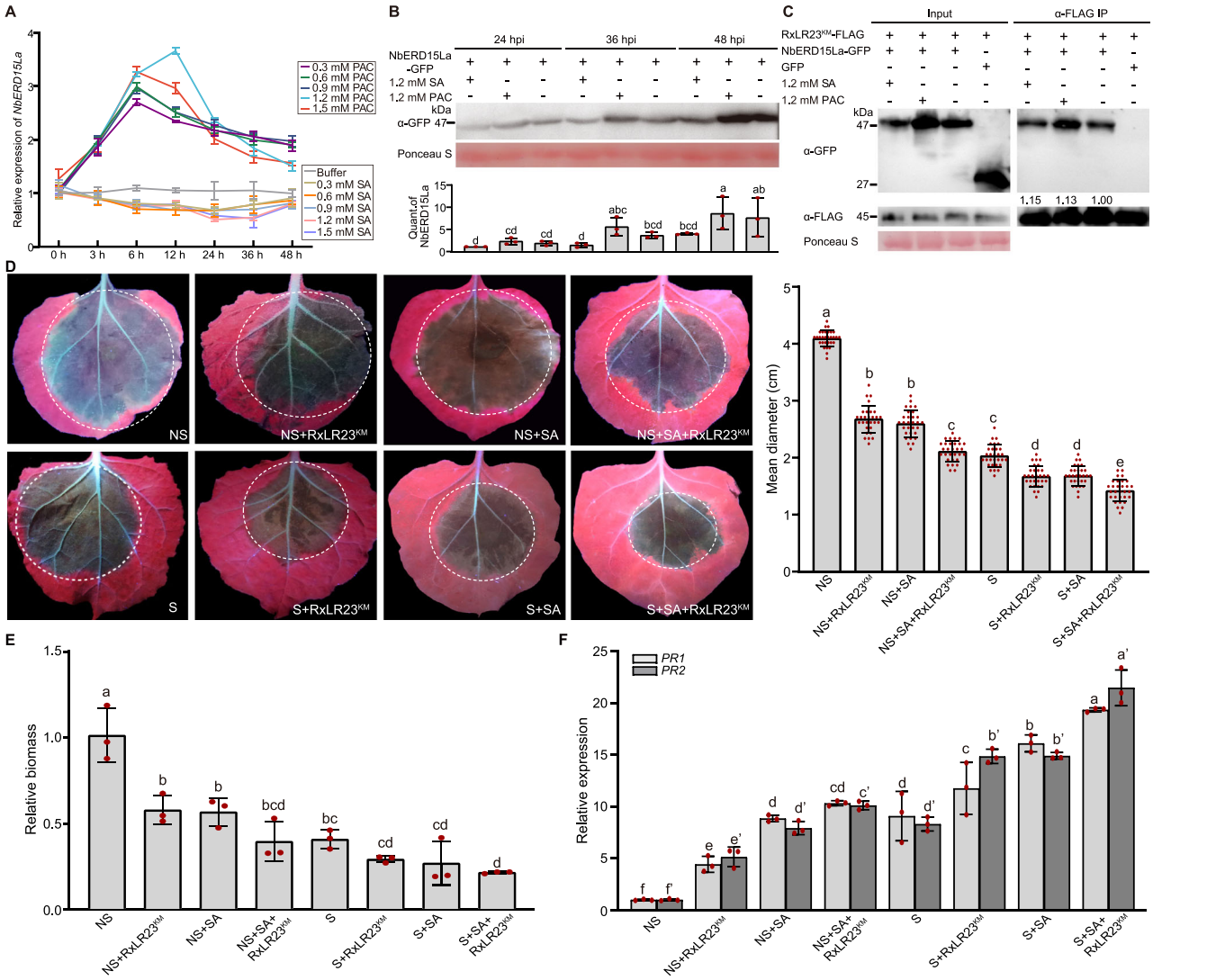

Fig. 6 | SA enhances RxLR23^{KM}-triggered plant defense response by suppressing ERD15La activity. The activity of NbERD15La was affected by SA or PAC. **A** Transcript levels of *NbERD15La* were measured by qRT-PCR after treatment with SA or PAC. Values are presented as mean ± SD, $n = 3$ independent experiments. **B** Expression of NbERD15La was detected using quantitative western blots in leaves following treatment with SA or PAC. Quantification of NbERD15La expression was calculated as relative intensity of NbERD15La bands. Protein loading is indicated by Ponceau S. Values are presented as mean ± SD, $n = 3$ independent experiments. **C** Neither SA nor PAC affected the interaction of RxLR23^{KM} with NbERD15La. Right panels showed expression (+) of NbERD15La-GFP, RxLR23^{KM}-FLAG, and GFP. Left panels showed the combination of RxLR23^{KM} and NbERD15La. The ratio of the band intensity of IP to input was shown in the bottom of IP panel. Equal protein loading was indicated by Ponceau S. **D**–**F** *N. benthamiana* treatment with single or sequential combinations of RxLR23^{KM} and SA in TRV:NbERD15La (S) or TRV:GFP (NS) plants. NS or S plants without any treatment were used as control. **D** Representative lesions were taken under UV irradiation at 48 h after *P. capsici* infection. Mean diameter of lesions was measured at 48 hpi. Values are presented as mean ± SD, $n = 30$ samples. **E** qPCR was used to measure the relative biomass on the ratios of *P. capsici* to S and NS leaves DNA at 48 hpi. The ratio of NS leaves without any treatment was assigned to value 1.0. Values are presented as mean ± SD, $n = 3$ independent experiments. **F** Expression levels of *PR1/2* was detected by qRT-PCR at 48 hpi. Values are presented as mean ± SD, $n = 3$ independent experiments. The data in (**B**, **D**–**F**) were analyzed by ANOVA one-way comparison followed by least significant difference (LSD) test and different letters above the bars indicate a significant difference at $p < 0.05$. *Pcβ-actin* and *NbEF1α* were identified as the most suitable reference genes for normalization in *P. capsici* and *N. benthamiana*, respectively. These experiments (**B**–**D**) were repeated three times. Source data are provided as a Source Data file.

Importantly, the various of ERD15La protein bands in Input was similar to those of in quantitative western blots under the treatment with SA or PAC (Fig. 6C). Together, the characteristics of ERD15La in plants are inhibited by spraying SA, suggesting that SA is possible to suppress ERD15La's effective conduction on RxLR23^{KM} to enhance plant defense responses.

To further validate whether SA can inhibit the activity of ERD15La to trigger plant immunity in response to ectopic expression of RxLR23^{KM}, the leaves of TRV:NbERD15La (Silenced, S) or TRV:GFP (Non-silenced, NS) *N. benthamiana* were ectopically expressed with RxLR23^{KM} and then were sprayed with 0.5 mM SA at 4–5 hpi[87] before inoculation with zoospores. We calculated the lesion size of S plants in comparison with NS plants in response to various treatments. As shown in Fig. 6D–F, the leaves of NS plants without any treatment produced the largest lesions size and maximum pathogen biomass, and defense responses were gradually increased in NS + RxLR23^{KM}, NS + SA, NS + SA + RxLR23^{KM}, respectively. In S plants, the treatments with RxLR23^{KM}, SA or SA + RxLR23^{KM} resulted in gradually reduced lesion size and pathogen biomass. Compared with NS leaves, silencing of NbERD15La visibly restricted both lesion expansion and pathogen biomass (Fig. 6D, E). These two indicators of plant defense responses were inversely correlated with expression levels of *PR1/2* (Fig. 6F). At

the same time, the plant defense responses in response to all various treatments in S and NS plants is correlated with the expression of *PR1/2* (Fig. 6F). Taken together, these results suggest that SA inhibit the activity of NbERD15La in response to conduction on RxLR23^{KM} triggers a plant defense response to *P. capsici* infection.

NbNAC68 activated plant defense response is blocked by NbERD15La

To identify the potential host interactors of NbERD15La, we transiently expressed NbERD15La in *N. benthamiana* and screened protein interactors using Co-immunoprecipitation (Co-IP) followed by liquid chromatography-tandem mass spectrometry (LC-MS/MS). We identified several proteins that potentially interacted with NbERD15La (Supplementary Data 1), in which three proteins contain a putative NAC domain-containing protein 68, named as NbNAC68a (NbL04g05300.1), NbNAC68b (NbL04g05300.1), and NbNAC68c (NbL18g07320.1), respectively. NAC protein is a member of a large family of transcription factors, and some of them mediate response to biotic and abiotic stresses[88]. NbNAC68a shares 70.65% and 95.21% identity with NbNAC68b and NbNAC68c, respectively. The high similarity among them prompted us to determine whether NbERD15La interacted with each of these three proteins. The Co-IP and LCI assays showed that NbERD15La interacted with NbNAC68a/b/c in vivo (Supplementary Fig. 15A, B). Then, we verified that RxLR23^{KM} did not interact with NbNAC68a/b/c by Co-IP and LCI assay (Supplementary Fig. 15C, D).

To determine if NbERD15La altered the subcellular localization of NbNAC68a/b/c, we observed the localization of NbNAC68a/b/c-mCherry in the presence or absence of NbERD15La-GFP in *N. benthamiana* leaves. Confocal images revealed that NbNAC68a/b/c-mCherry localized to the cytoplasm and nucleoplasm, which was not changed at the presence of NbERD15La-GFP (Supplementary Fig. 16A, B). In cells where both fluorescent proteins were expressed, we measured the fluorescence intensity of mCherry and GFP along a transect bisecting the nucleus. Fluorescence intensity of NbNAC68a/b/c-mCherry was closed to that of NbERD15La-GFP in nucleoplasm (Supplementary Fig. 16C) Thus, NbERD15La did not alter the distribution of NbNAC68a/b/c in the plant cell.

Since NbNAC68a/b/c interacts with NbERD15La, we examined the expression patterns of *NbNAC68a/b/c* in *N. benthamiana* leaves following inoculation with *P. capsici* zoospores at multiple time points by qRT-PCR, respectively (Supplementary Fig. 17A). In contrast to 0 hpi, transcript expression of *NbNAC68a/b/c* appears in all treated time points after *P. capsici* infection, but it produced strong expression levels from 1.5 to 72 hpi with a spike at 6 hpi. Thus, *NbNAC68a/b/c* is typically activated at early stages of infection, but notably this spike of *NbNAC68a/b/c* expression occurs later than the peak expression of *RxLR23* or *NbERD15La* (Supplementary Figs. 1 and 12A). To further investigate the roles of NbNAC68a/b/c in plant immunity, NbNAC68a/b/c was singly expressed or co-expressed in *N. benthamiana* leaves and subsequently inoculated with *P. capsici* zoospores at 24 h, respectively. Single expressing or co-expressing NbNAC68a/b/c resulted in obviously reduced lesion sizes, decreased pathogen biomass, and strongly increased expression of *PR1/2* relative to GFP at 48 hpi (Supplementary Fig. 17B–D). In contrast to each of NbNAC68, co-expression of NbNAC68a/b/c triggered slightly increased resistance to *P. capsici* infection. Thus, NbNAC68a/b/c co-efficiently contributes to activating plant immunity. To further address the role of these three genes related to plant immunity, *NbNAC68a/b/c* was simultaneously knocked down in *N. benthamiana* by VIGS. Transcription levels of *NbNAC68a/b/c* were reduced in TRV: NbNAC68a/b/c by 60% to 70% relative to TRV:GFP (Supplementary Fig. 17E). TRV:NbNAC68a/b/c plants showed a slightly stunted phenotype compared with TRV:GFP plants, but TRV:PDS leaves were obviously bleached in color (Supplementary Fig. 17F). The leaves of TRV:NbNAC68a/b/c and TRV:GFP plants were then inoculated with *P. capsici* zoospores. Silencing of *NbNAC68a/b/c* accelerated *P. capsici* development compared with unsilenced plants (Supplementary Fig. 17G), which was associated with significantly enlarged lesion diameter, increased pathogen biomass and decreased expression levels of *PR1/2* (Supplementary Fig. 17G–I). All these results suggested that NbNAC68a/b/c positively regulated plant immunity.

To detect whether NbERD15La is required for NbNAC68a/b/c-triggered plant immunity, TRV:NbERD15La (S) and TRV:GFP (NS) leaves were transiently co-expressed with NbNAC68a/b/c and subsequently inoculation with *P. capsici* zoospores. Interestingly, co-expression of NbNAC68a/b/c in S or NS leaves led to obviously decreased pathogen growth and pathogen biomass relative to expression of GFP in S or NS leaves at 48 hpi, respectively (Fig. 7A–C), while co-expression of NbERD15La with NbNAC68a/b/c in S and NS leaves resulted in increased lesion size and *P. capsici* biomass compared with those of expressing NbNAC68a/b/c (Fig. 7A, B). All these results are consistent with the expression patterns of *PR1/2* upon above corresponding treatments (Fig. 7C). Thus, NbNAC68a/b/c activated plant immunity is blocked by NbERD15La. Then, we examined the levels of SA and ABA by HPLC-MS in TRV:NbERD5La and TRV:GFP plants after all above treatments. As a result, transient co-expression of NbNAC68a/b/c increased SA content and reduced ABA content at 24 h, while this patterns of SA and ABA was disturbed after co-expressing NbERD15La with NbNAC68a/b/c in TRV:NbERD5La and TRV:GFP plants (Fig. 7D, E). Each protein size was verified by western blot using GFP-antibodies in silenced and non-silenced leaves (Fig. 7F). Therefore, plant immunity triggered by NbNAC68 is blocked by NbERD15La.

To further demonstrate whether the functions of NbERD15La is correlated with NbNAC68a/b/c-triggered plant immunity, TRV:NbERD15La-NAC68a/b/c, TRV:NbNAC68a/b/c, and TRV:NbERD15La *N. benthamiana* plants were obtained using VIGS. TRV:GFP *N. benthamiana* was as control. Transcription levels of *NbERD15La/NbNAC68a/b/c* in TRV:NbERD15La-NAC68a/b/c plants, of *NbERD15La* in TRV:NbERD15La plants, and of *NbNAC68a/b/c* in TRV:NbNAC68a/b/c plants were reduced by 55% to 70% relative to TRV:GFP (Supplementary Fig. 18A). The TRV:NbERD15La-NAC68a/b/c, TRV:NbNAC68a/b/c, and TRV:NbERD15La plants appeared slightly stunted phenotype compared with TRV:GFP plants, while TRV:PDS leaves exhibited chlorophyll bleaching (Supplementary Fig. 18B). The leaves of TRV:NbERD15La-NAC68a/b/c, TRV:NbNAC68a/b/c, TRV:NbERD15La and TRV:GFP were then inoculated with *P. capsici* zoospores alone. Silencing of *NbERD15La* significantly inhibited *P. capsici* development compared with TRV:GFP leaves, which was correlated with reduced lesion diameter and pathogen biomass, and increased expression levels of *PR1/2* (Supplementary Fig. 18C–E). In contrast, co-silencing *NbERD15La-NAC68a/b/c* or co-silencing *NbNAC68a/b/c* accelerated *P. capsici* colonization compared with TRV:GFP leaves along with obviously enlarged lesion diameter, increased pathogen biomass and decreased expression levels of *PR1/2* (Supplementary Fig. 18C–E). These results indicate that NbERD15La is a potential negative regulator of NAC68a/b/c-triggered plant immunity, restraining the activity of NbERD15La result in motivating NbNAC68a/b/c to promote immune response.

To investigate how NbERD15La inhibition of NbNAC68a/b/c triggered-plant immunity, we next examined whether NbNAC68a/b/c can directly bind to *PR1/2* promoter region. EMSA experiments indicate that NbNAC68a/b/c directly binds to the *PR1/2* promoter region (Supplementary Fig. 19A). In the reporter construct, we cloned *PR1/2* promoter to the upstream of the firefly luciferase reporter gene LUC (Supplementary Fig. 19D) and carried out a dual-luciferase reporter assay by co-expressing the reporter and effector constructs in *N. benthamiana* leaves. The initial qualitative assay showed activation of LUC reporter gene in presence of NbNAC68a/b/c (Supplementary Fig. 19E). To verify this result in a highly sensitive quantitative assay, we

https://doi.org/10.1038/s41467-024-50782-3

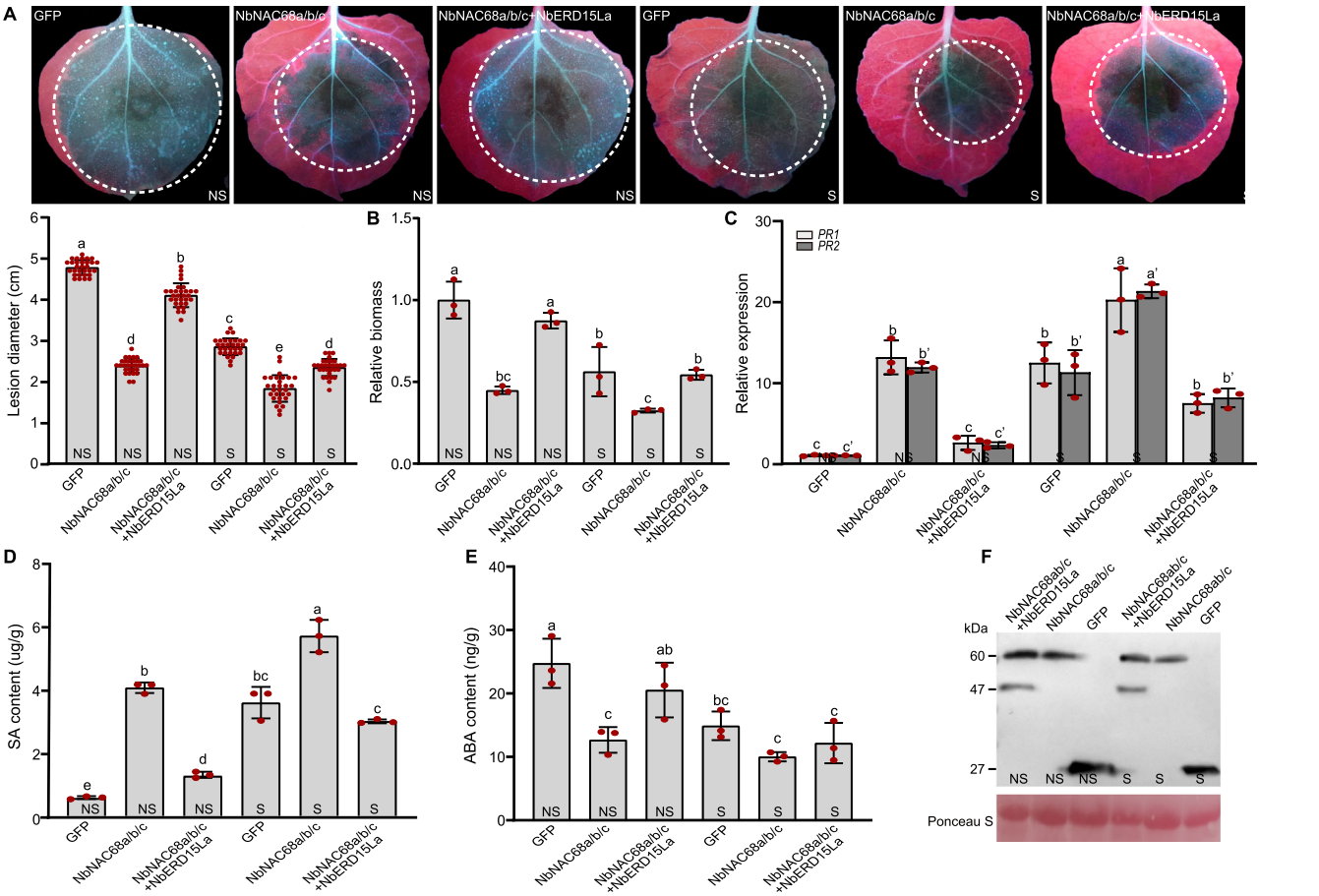

Fig. 7 | NbERD15La negatively regulated NbNAC68a/b/c-triggered plant defense response to *P. capsici* infection. pBinGFP2:NbNAC68a/b/c, pBinGFP2:NbERD15La, and pBinGFP2 were transiently expressed in *N. benthamiana* leaves alone, while NbERD15La + NbNAC68a/b/c is transiently co-expressed in *N. benthamiana* leaves. S represents TRV:NbERD15La *N. benthamiana* (Silenced plants). NS represents TRV:GFP *N. benthamiana* (Non-silenced plants). All tested *N. benthamiana* leaves were inoculated with *P. capsici* zoospores after expression of the corresponding constructs at 24 h. **A** Typical lesion images of leaves were photographed under UV irradiation at 48 hpi. Mean diameter of lesions was calculated at 48 hpi. Values are presented as mean ± SD, $n = 30$ samples. **B** Relative biomass of *P. capsici* was measured by qPCR at 48 hpi. *Pcβ-actin* and *NbEF1α* were identified as the most suitable reference genes for normalization. The ratio in NS leaves inoculated with GFP was assigned to value of 1.0. Values are presented as mean ± SD, $n = 3$ independent experiments. **C** Expression levels of *PR1/2* were detected by qRT-PCR at 48 hpi. *NbEF1α* of *N. benthamiana* was used as constitutively expressed endogenous control. Values are presented as mean ± SD, $n = 3$ independent experiments. **D**, **E** The variations of SA or ABA content were examined by HPLC-MS in *N. benthamiana* leaves after above treatments at 24 hpi. Values are presented as mean ± SD, $n = 3$ independent experiments. **F** Expected protein sizes were detected by western blots using GFP-antibodies alone. Protein loading is indicated by Ponceau staining (Ponceau S). The data in Fig. 6A–E were analyzed by ANOVA one-way comparison followed by least significant difference (LSD) test and different letters above the bars indicate a significant difference at $p < 0.05$. These experiments (**A**, **F**) were repeated three times with similar results. Source data are provided as a Source Data file.

measured relative luminescence. The luminescence ratio increased significantly in presence of NbNAC68a/b/c. Therefore, NbNAC68a/b/c is a strong factor for the transcriptional regulation of NbNAC68a/b/c. Subsequent, EMSA and dual-luciferase experiments confirm NbERD15La can impair binding of NbNAC68a/b/c and *PR1/2* promoter (Supplementary Fig. 19B) and inhibit activity of *PR1/2* promoter activated by NbNAC68a/b/c alone (Supplementary Fig. 19E). Thus, NbERD15La negatively regulated plant immunity which is likely to correlate with these two characteristics of NbERD15La act on NbNAC68a/b/c and *PR1/2* promoter. In summary, NbNAC68a/b/c positively regulated plant immunity. NbERD15La is an upstream regulator of NAC68a/b/c and negatively regulated NAC68a/b/c-triggered plant immunity.

RxLR23^{KM} impairs the interaction of ERD15La with NbNAC68a/b/c

Prior work showed that transcription factor NAC6 could induce an NRP-mediated cell death signaling pathway[89]. To further investigate whether RxLR23^{KM} triggers cell death and plant immunity correlated with NbNAC68a/b/c, pBinGFP2:RxLR23^{KM}, pBinGFP2:RxLR23^{RM}, pBinGFP2:RxLR23^{RR}, pBinGFP2:INF1, and pBinGFP2 were transiently expressed in TRV:NbNAC68a/b/c and TRV:GFP leaves, respectively. pBinGFP2:INF1 and pBinGFP2 were used as positive and negative controls, respectively. In contrast to RxLR23^{RM} and RxLR23^{RR}, the cell death caused by RxLR23^{KM} was significantly decreased, along with the reduced percentage of necrosis and electrolyte leakage in TRV:NbNAC68a/b/c leaves compared with in TRV:GFP leaves, indicating that NbNAC68a/b/c is required for RxLR23^{KM} to trigger cell death (Supplementary Fig. 20A–C). In addition, TRV:NbNAC68a/b/c and TRV:GFP leaves were expressed with RxLR23^{KM}, RxLR23^{RM}, RxLR23^{RR}, and GFP and then infected by *P. capsici* zoospores at 24 h. Expression of RxLR23^{KM} promoted *P. capsici* colonization, and increased pathogen biomass in TRV:NbNAC68a/b/c leaves relative to TRV:GFP leaves (Supplementary Fig. 20D, E). Furthermore, DAB staining showed that RxLR23^{KM} triggered ROS accumulation was significantly attenuated in TRV:NbNAC68a/b/c leaves compared with in TRV:GFP leaves (Supplementary Fig. 20F). All these data are opposed to those of RxLR23^{RM} and RxLR23^{RR} in TRV:NbNAC68a/b/c and TRV:GFP leaves, respectively.

https://doi.org/10.1038/s41467-024-50782-3

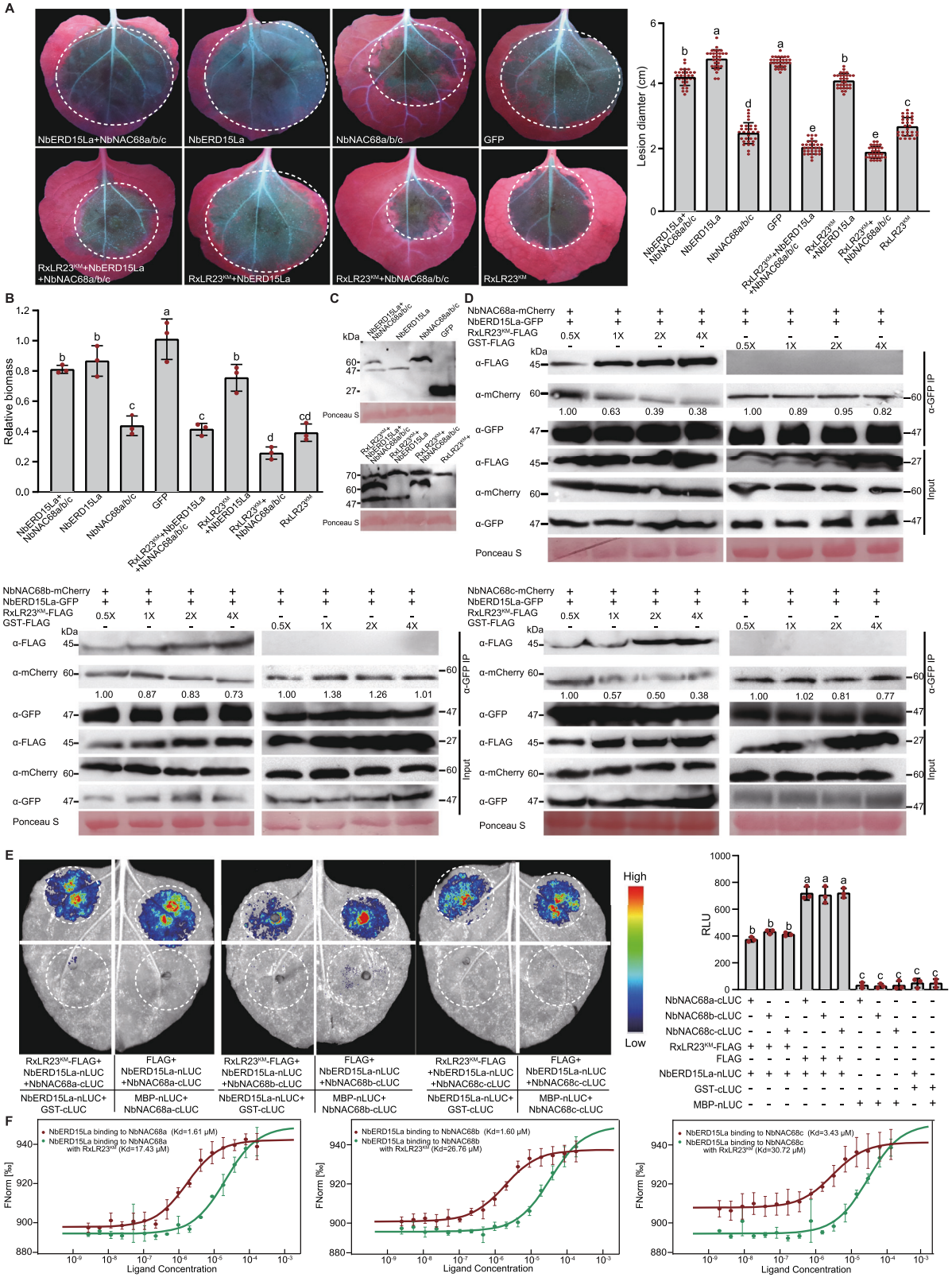

Therefore, RxLR23^{KM} induced cell death and plant defense response is mediated by NbNAC68/a/b/c, while the slight cell death and defence response caused by RxLR23^{RM} and RxLR23^{RR} are not co-related with NbNAC68/a/b/c. In order to address whether NbNAC68a/b/c is necessary for RxLR23^{KM} triggered- and NbERD15La-regulated plant immunity, we transiently expressed NbERD15La, RxLR23^{KM} combination with NbERD15La, and GFP in TRV:NbNAC68a/b/c leaves preceded inoculation with *P. capsici* zoospores. Significantly, single expression of GFP, RxLR23^{KM} or co-expression of RxLR23^{KM} and NbERD15La in silenced leaves resulted in larger lesion diameter and pathogen biomass than in unsilenced leaves, respectively (Supplementary Fig. 21A, B). In contrast to unsilenced leaves, single expression of GFP, RxLR23^{KM} or co-expression of RxLR23^{KM} and NbERD15La reduced SA and increased ABA levels in the silenced leaves at 24 h (Supplementary

Fig. 8 | RxLR23^{KM} impairs the interaction of ERD15La and NbNAC68a/b/c to trigger plant defense against *P. capsici* infection. A, **B** pBinGFP2:RxLR23^{KM}, pBinGFP2:NbERD15La, pBinGFP2:NbNAC68a/b/c, pBinGFP2:NbERD15La + pBinGFP2:NbNAC68a/b/c, pBinGFP2:RxLR23^{KM} + pBinGFP2:NbERD15La, pBinGFP2:RxLR23^{KM} + pBinGFP2:NbNAC68a/b/c, pBinGFP2:RxLR23^{KM} + pBinGFP2:NbERD15La + pBinGFP2:NbNAC68a/b/c, or pBinGFP2:GFP was transiently expressed in *N. benthamiana* leaves and subsequently inoculated with *P. capsici* zoospores at 24 hpi. **A** Representative lesions were taken under UV irradiation at 48 hpi ($n = 30$ samples). Mean diameter of lesions was measured at 48 hpi. Values are presented as mean ± SD. **B** Relative biomass of *P. capsici* was measured by qPCR at 48 hpi. *Pcβ-actin* and *NbEF1α* were identified as the most suitable reference genes for normalization. The ratio in the leaves inoculated with GFP was assigned to value of 1.0. Values are presented as mean ± SD, $n = 3$ independent experiments. **C** Expected protein sizes were detected by western blot. Protein loading is indicated by Ponceau S. **D** RxLR23^{KM} attenuates interaction of ERD15La and NbNAC68a/b/c. NbNAC68a/b/c-mCherry and NbERD15La-GFP were transiently co-expressed in *N. benthamiana* leaves along with increasing amounts of RxLR23^{KM}-FLAG or GST-FLAG. The ratio of NbNAC68a/b/c or RxLR23^{KM} immunoprecipitated by NbERD15La to their expression quantity was assigned to value 1.0 when NbNAC68a/b/c or NbERD15La with RxLR23^{KM} or GST were co-expressed into leaves in a 1:1:0.5 ratio. Equal protein loading is indicated by Ponceau S. **E** RxLR23^{KM} impairs NbNAC68a/b/c interaction with NbERD15La by LCI. MBP-nLUC and GST-cLUC were used as controls. RxLR23^{KM} and fusion proteins were co-expressed in leaves. Images were obtained at 2 days. LCI was evaluate interaction of NbERD15La with NbNAC68a/b/c in presence or absence of RxLR23^{KM}. Relative luminescence units (RLUs) were used to measure the luminous intensity. Values are presented as mean ± SD, $n = 3$ independent experiments. **F** RxLR23^{KM} weakens binding affinity of NbERD15La with NbNAC68a/b/c by MST. Values are presented as mean ± SD, $n = 3$ independent experiments. The data were analyzed by ANOVA one-way comparison followed by least significant difference (LSD) test. Different letters above the bars indicate a significant difference at $p < 0.05$. The experiments were repeated three times with similar results. Source data are provided as a Source Data file.

Fig. 21C, D). All these results were correlated with the expression patterns of *PR1/2* in silenced and unsilenced leaves by varying challenges (Supplementary Fig. 21E). Thus, NbNAC68a/b/c is a downstream regulator of NbERD15La and positively regulated plant immunity.

These experiments confirmed that NbERD15La negatively regulated RxLR23^{KM} or NbNAC68a/b/c-triggered plant immunity. To further illustrate how the combinations of RxLR23^{KM}, NbERD15La, and NbNAC68a/b/c regulate plant immunity mediated by RxLR23^{KM}, NbERD15La, and NbNAC68a/b/c after separately, pairwise, or simultaneously expressing in *N. benthamiana* leaves. Co-expression of RxLR23^{KM} with NbNAC68a/b/c resulted in the smallest lesion diameter and the least *P. capsici* biomass (Fig. 8A, B). The lesion area and *P. capsici* biomass caused by co-expression of RxLR23^{KM}, NbNAC68a/b/c and NbERD15La were close to those of expressing RxLR23^{KM} and NbNAC68a/b/c alone, while co-expression of NbERD15La with RxLR23^{KM} or NbNAC68a/b/c produced the similar lesion size and pathogen biomass with expression of NbERD15La or GFP (Fig. 8A, B). Each protein size was verified by western blot using GFP-antibodies in *N. benthamiana* leaves (Fig. 8C). Thus, NbERD15La blocks the NbNAC68a/b/c activation in RxLR23^{KM}-triggered plant immune pathway. To further test whether NbERD15La plays a central role in this defense pathway, the interactions of NbERD15La, NbNAC68a/b/c, and RxLR23^{KM} were assayed using Co-IP. Expression of RxLR23^{KM} was gradually increased in *N. benthamiana* leaves that resulted in weak interaction of NbNAC68a/b/c with NbERD15La, and reinforced combination of RxLR23^{KM} with NbERD15La (Fig. 8D). Thus, expression of RxLR23^{KM} impairs the intensity of NbNAC68a/b/c interaction with NbERD15La. Then, LCI and MST assays showed that the binding intensity of NbNAC68a/b/c with NbERD15La was lower than that of RxLR23^{KM} with NbERD15La (Supplementary Fig. 22A), in which the order of their binding affinity is gradually decreased as follows: NbERD15La with RxLR23^{KM}, NbERD15La with NbNAC68a, NbERD15La with NbNAC68b, and NbERD15La with NbNAC68c (Supplementary Fig. 22B). Thus, RxLR23^{KM} shows higher affinity to NbERD15La than that of NbERD15La with NbNAC68a/b/c. Together, co-expression of RxLR23^{KM} with both NbERD15La and NbNAC68a/b/c resulted in impairing the interactions of NbERD15La with NbNAC68a/b/c alone (Fig. 8D–F). Therefore, over-expression of RxLR23^{KM} contributed to NbNAC68a/b/c divorcing from NbERD15La. In addition, the evidence of EMSA and dual-luciferase assays further demonstrated that RxLR23^{KM} contributed to attenuating NbERD15La to inhibit the activity of NbNAC68a/b/c with *PR1/2* promoter (Supplementary Fig. 19C, E). All these results indicate that NbERD15La is a central regulator in this pathway, in which RxLR23^{KM} impairs NbERD15La interaction with NbNAC68a/b/c. Furthermore, NbNAC68a/b/c is a consequence of the binding of RxLR23^{KM} to ERD15La and plays a vital role in the cell death and plant immunity response.

In addition, we evaluated whether RxLR23^{KM} alters the subcellular localization of NbERD15La and NbNAC68a/b/c in *N. benthamiana* leaves alone. Upon co-expression of RxLR23^{KM}-Flag with both NbERD15La-GFP and NbNAC68a/b/c-mCherry in *N. benthamiana*, confocal images showed that NbERD15La or NbNAC68a/b/c localized to the cytoplasm and nucleoplasm, consistent with the absence of RxLR23^{KM} (Supplementary Fig. 23A, B). We measured the fluorescence intensity of GFP and mCherry along a transect bisecting the nucleus in plant cells. Fluorescence intensity of NbERD15La-GFP was closed to NbNAC68a/b/c-mCherry (Supplementary Fig. 23C), indicating NbERD15La and NbNAC68a/b/c accumulated in the nucleoplasm in the presence or absence of RxLR23^{KM}. Thus, RxLR23^{KM} does not alter the distribution of NbERD15La and NbNAC68a/b/c in the plant cell, suggesting that RxLR23^{KM} interacts with NbERD15La to motivate NbNAC68a/b/c-triggered the cell death and plant immunity in the cytoplasm and nucleoplasm.

Discussion

P. capsici genome, as well as *P. infestans* and *P. sojae*, has a large number of secreted RxLR effectors that are delivered into host tissues[17–19]. RxLR23 was originally identified as an effector from an aggressive *P. capsici* on *C. annuum*. Two allelic variants (RxLR23^{RM} and RxLR23^{RR}) of RxLR23 from two less virulent isolates differed from RxLR23^{KM} at two amino acid positions (K^{93} and M^{320}) (Supplementary Fig. 4). RxLR23 was first verified as a crucial effector for *P. capsici* virulence (Fig. 1) and is one of four recently characterized *P. capsici* RxLR effectors that are associated with a cell death response (Fig. 2)[33,76]. Expression of RxLR23^{KM} and its allelic variants inhibited the progress of *P. capsici* infection, and triggered production of varying amounts of ROS and alterative expressions of *PR1/2* (Fig. 3). Over-expression of PcAvr3a or PcAvh1 resulted in enhanced virulence[76,90], while expression of RxLR23 and RxLR207[33] inhibited *P. capsici* infection. The timing of expressing these four genes is important for their roles in pathogen virulence. The early expression of PcAvh1 is attributed to its essential role as a virulent factor, while a second peak at 36 hpi is hypothesized to contribute to the switch to necrotrophy[76]. Expression of RxLR207 at 9 hpi is also suggested to promote the transition from biotrophy to necrotrophy in host tissues[33]. Since constitutive expression of RxLR23 impairs rather than promotes infection, this may explain why RxLR23 is only transiently expressed at the start of the infection. At later time periods, expression of RxLR23 may be limited to the leading edges of hyphal ingress to avoid activating the layered defense of plant cells[91]. The localization of RxLR effectors in plant cells is often correlated with their functions[80]. RxLR23^{KM} localizes in the cytoplasm and nucleus (Supplementary Fig. 3D) with an additional localization to the nucleolus. The nucleolus plays a central role in the regulation of plant

development and responses to abiotic and biotic stresses[92]. RxLR23^{KM} is clearly localized to nucleolus in contrast to RxLR23^{RM} and RxLR23^{RR} (Supplementary Fig. 5), which is certainly suggestive of resulting in varying roles in plant response. RxLR23^{KM} elicited a stronger cell death than RxLR23^{RM} and RxLR23^{RR} in *N. benthamiana* leaves (Fig. 2). In contrast to these alleles, expression of RxLR23^{KM} also significantly inhibited *P. capsici* infection (Fig. 3). Moreover, transgenic lines of RxLR23^{KM} showed highly resistant to *P. capsici* compared with two alleles (Supplementary Fig. 7).

In addition, RxLR23^{KM}, RxLR23^{RM}, or RxLR23^{RR} significantly affected the growth and development of *Arabidopsis* (Supplementary Fig. 6), which was likely attributed to RxLR23 binding to other host proteins involved in plant development, secreting toxin to disturb plant cell, and even modulating plant hormone levels, similar to previous studies[6,93]. Previous studied reported that two alleles of AVR3a (AVR3a^{KI} and AVR3a^{EM}) from *P. infestans* carried out antipodal functions on detection of R3a, suppression of INF1-triggered cell death, and triggering ETI[29,94]. In this study, the functions of RxLR23^{KM} show obvious advantage over RxLR23^{RM} or RxLR23^{RR} in *N. benthamiana*. We speculate the main reasons for the unique features of RxLR23 as follows: (1) The interaction of RxLR23^{KM} with host's target protein regulated by K^{93} (Lysine) M^{320} (Methionine) that is likely to be attenuated by R^{93} (Arginine) and R^{320} (Arginine); (2) The modification or side length of these two key amino acids (Lysine or Methionine) is likely to distinguish from Arginine. However, how a few crucial amino acids influence the function of a full-length sequence need to be further investigated.

Our experiments found that RxLR23^{KM} specifically interacted with ERD15La (Fig. 4 and Supplementary Fig. 9). Moreover, NbERD15La localized to the cytoplasm and nucleus (Supplementary Fig. 10), while RxLR23^{KM} localized to the cytoplasm, nucleus, and nucleolus. Co-expression of RxLR23^{KM} and NbERD15La did not result in a shift of NbERD15La to the nucleolus. Thus, RxLR23^{KM} and NbERD15La co-localized to cytoplasm and nucleoplasm. Moreover, $_{NLS}$RxLR23^{KM} triggered a stronger plant cell death response than $_{NES}$RxLR23^{KM} (Supplementary Fig. 3), while the interaction of NbERD15La with $_{NES}$RxLR23^{KM}, or $_{NLS}$RxLR23^{KM} was slightly weakened compared with RxLR23^{KM} (Supplementary Fig. 11). Because ERD15 proteins contain an evolutionarily conserved motif, named as PAM2 which enables ERD15 interact with Polyadenylate Binding Proteins (PABP)[95]. We noted a diminished cell death response in $_{NES}$RxLR23^{KM} lesions and enhanced cell death response in $_{NLS}$RxLR23^{KM} lesion sites (Supplementary Fig. 3), which is likely due to the binding of ERD15La with RxLR23^{KM} interferes with the translation of many proteins. All these results suggest that RxLR23^{KM}-triggered cell death might be mediated by other proteins that distributed in cytoplasm, nucleus, and nucleolus. *In planta* effectoromics screening indicates that many RxLR effectors may have multiple targets[96]. Thus, we cannot exclude the possibility that RxLR23^{KM} may interact with other proteins in either the cytoplasm or nucleus.

ERD15 proteins can be induced by low temperatures[50], abscisic acid (ABA)[82], drought and salinity[97], and biotic stress stimuli[48]. Our experiments found that *NbERD15La* could response to *P. capsici* infection (Supplementary Fig. 12A). Moreover, silencing *NbERD15La* resulted in enhancing plant immunity (Fig. 5A, C, D and Supplementary Fig. 12F, G), opposing to over-expressing ERD15 improved plant resistance to the bacterial pathogen *Erwinia caratova*[50], which might be due to diversification in function among the members of ERD15 family. Furthermore, expression of NbERD15La inhibited RxLR23^{KM}-triggered plant immunity (Fig. 5), suggesting that NbERD15La is a negative regulator of plant immunity. Prior work showed that ERD15L down-regulated the response to ABA, while activating SA-dependent defense genes[50]. In our experiments, silencing of *NbERD15La* resulted in high baseline levels of SA and low levels of ABA (Fig. 5H, I). As a regulator of SA, ERD15La is a potential target of effectors, which is certainly expected to activate a layered defense response. Some RxLR effectors bind target proteins to enhance strong ROS response for plant resistance[33]. Expression of RxLR23^{KM} promoted ROS burst in TRV:NbERD15La or TRV:GFP *N. benthamiana*. However, the ROS response was significantly enhanced in TRV:NbERD15La plants compared with TRV:GFP plants (Fig. 5B, E), suggesting that silencing NbERD15La sensitized the cells to exogenous signals.

Several effectors have been reported to target genes regulating the SA pathway. In addition to targeting Med19a[40], *H. arabidopsidis* effector HaRxL06 targets Radical-Induced cell death to suppress SA-induced genes[44], but the mechanism of SA signaling suppression is still unknown. *P. sojae* delivers Pslsc1 into the host cytoplasm where it hydrolyzes isochorismate to prevent SA synthesis[41]. *P. infestans* delivers Pi04314 into the host nucleus causing the relocation of three PP1c isoforms out of the nucleolus and disrupting SA synthesis[80] Because of the central importance of SA signaling to plant defense against biotrophic pathogens, we compared the defense responses to spraying with SA and expression of RxLR23^{KM} in S (TRV:NbERD15La) and NS (TRV:GFP) plants. SA spraying in S or NS plants impaired the progress of infection (Fig. 6D–F). In addition, Spraying SA can reduce the expression levels of *NbERD15La* compared with treatment with PAC (a potential inhibitor of SA biosynthesis) in *N. benthamiana* (Fig. 6A, B). SA could induce the expression of pathogenesis-related proteins[98,99], but ERD15La, as a negative regulator of plant immunity, is down-regulated by SA treatment. Thus, SA was likely to deploy other components or trigger a signaling pathway to interfere the expression of ERD15L. However, the exact mechanism of this issue is still unknown.

NbERD15La is a negative regulator of RxLR23^{KM}-triggered plant immunity. Silencing of NbERD15La increased the expression levels of *PR1/2* under various treatments. A much stronger inhibition of infection was observed in S plants challenged with RxLR23^{KM}, or SA and RxLR23^{KM} and increased expression levels of *PR1/2* relative to NS plants. Due to the buffering nature of the plant immune response, it has been postulated that pathogens would need to blanket the entire signaling network to avoid triggering plant defenses caused by targeting a central regulator[91]. To the best of our knowledge, our studies confirmed that a RxLR effector targeting ERD15L to circumvent the defense strategy of a nested defense system in plants.

To address how RxLR23^{KM}-NbERD15La complexes trigger plant immune response, our experiments confirmed that NbNAC68 interacted with NbERD15La alone rather than with RxLR23^{KM} (Supplementary Fig. 15). Notably, NbNAC68 could trigger plant defense response (Supplementary Fig. 17) and this function was blocked by NbERD15La (Fig. 7). Our data suggest that the NbERD15La-NbNAC68 complex inhibited the binding of NbNAC68 to *PR1/2* promoter regions and its activation of *PR1/2* gene expression (Supplementary Fig. 19). In addition, silencing of *NbERD15La* significantly inhibited *P. capsici* development, but co-silencing *NbERD15La-NbNAC68a/b/c* or co-silencing *NbNAC68a/b/c* accelerated *P. capsici* colonization (Supplementary Fig. 18C, D). Together, NbERD15La is an upstream regulator of NbNAC68 and negatively regulated NbNAC68-triggered plant immunity. Silencing *NbNAC68* resulted in reduced cell death, plant defense responses and H_2O_2 accumulation triggered by RxLR23^{KM} (Supplementary Fig. 20), indicating that NbNAC68 is an essential activator of this defense pathway. Activated NbNAC68a/b/c rather than a NbERD15La-NbNAC68a/b/c complex strongly mediated the defense responses triggered by RxLR23^{KM} (Fig. 8A). Interestingly, the binding intensity or affinity of NbNAC68a/b/c with NbERD15La was lower than that of RxLR23^{KM} with NbERD15La (Fig. 8D–F and Supplementary Fig. 22). Thus, the high expression of RxLR23^{KM} can block the binding of NbERD15La to NbNAC68a/b/c. Notably, co-expression of RxLR23 with NbERD15La and NbNAC68a/b/c in *N. benthamiana* leaves resulted in the reduced binding affinities of NbERD15La with NbNAC68a/b/c in various degrees, respectively (Fig. 8D–F), indicating that other proteins might be involved in the interactions of ERD15La with NAC68a/b/c, which need to be further investigated in the follow-up study. The release of NbNAC68 can

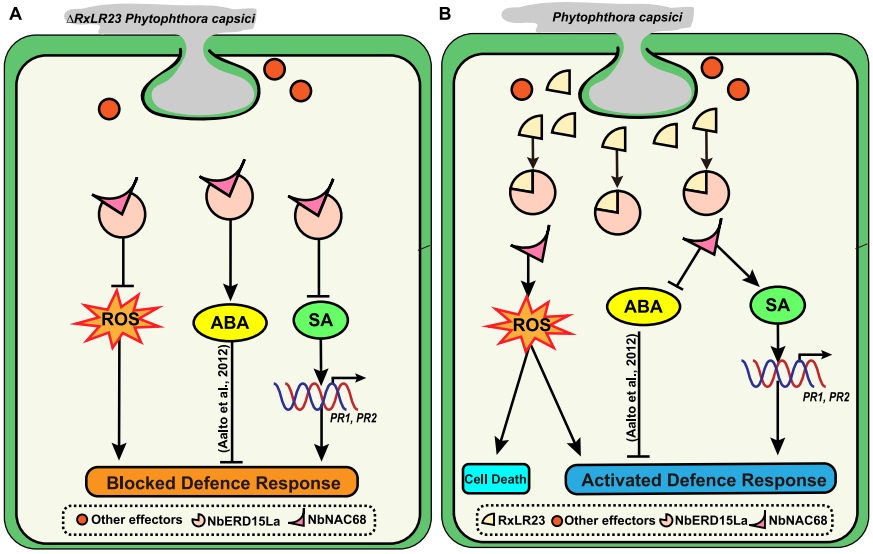

Fig. 9 | Model of *P. capsici* effector RxLR23 competitive binding to NbERD15La with NbNAC68 to activate plant defense response. Working model illustrating how RxLR23 manipulates the NbERD15La-NbNAC68 subcomplex to activate plant defense response. **A** In the absence of RxLR23, the activity of NbNAC68 is restricted by binding with NbERD15La following suppresses ROS and SA production and enhances ABA accumulation, leading to blocked plant defense response. **B** In the presence of RxLR23, NbNAC68 is released from NbERD15La-NbNAC68 complex, which increases SA and ROS accumulation, and reduces ABA production, resulting in enhanced plant defense response and cell death.

promote the expression of *PR1/2*. In this study, we find a novel defence pathway that NbERD15La as a central regulator coordinates RxLR23^{KM} to regulate NbNAC68-triggered plant immunity.

Since ERD15La is a negative regulator of ABA signaling, transient inhibition of ERD15La may contribute to infection by the release of ABA signaling[50,100]. In general, ABA is a negative regulator of oomycete pathogenesis[101] and other biotrophic pathogens[100]. ABA acts by depressing SA biosynthesis and signaling to compromise plant immunity[85,102]. In our experiments, ectopic expression of NbNAC68 and RxLR23^{KM} down-regulated ABA levels and enhanced plant immunity, but this effect was negated by over-expressing NbERD15La (Figs. 5I and 7E), but how down-regulation of ABA signaling promotes plant immunity is not fully understood.

Our research findings can be summarized as follows: RxLR23 is an essential effector, and in the absence of this effector there no successful infection. RxLR23^{KM} is strongly expressed only at the start of infection, but this transient expression of RxLR23^{KM} is sufficient to convert it from a weak to a very aggressive pathogen. In the absence of RxLR23^{KM}, the ERD15La-NbNAC68 complex causes NbNAC68 to be the rest state which inhibits ROS and SA accumulation and enhances ABA production, resulting in a blocked defense response (Fig. 9A). When RxLR23^{KM} is delivered into the plant cells at the earliest stages of infection, RxLR23^{KM} disturbs NbNAC68 binding to NbERD15La, incurring NbNAC68 to be activated. Activated NbNAC68 enhances the activity of SA signaling pathway, promotes ROS accumulation, and negatively regulates ABA signaling, thus, limiting the pathogen to successful infection. In addition, our experiment showed that RxLR23^{KM}, as well as *P. sojae* Avh241[103], *P. infestans* PexRD2[27] and PITG_22798[104], and *Plasmopara viticola* PvRXLR16[105], could induce cell death. Meanwhile, silencing NbNAC68 resulted in reduced cell death caused by RxLR23^{KM}, indicating that NbNAC68 is required for RxLR23^{KM}-triggered cell death. As previously noted, the localization of RxLR23 to the cytoplasm is also critically important. However, how NbNAC68 mediates cell death caused by RxLR23^{KM} need to be further investigated. In summary, RxLR23^{KM} is required for full virulence of *P. capsici*. Transient expression of RxLR effector prevents immune receptors[1], while constitutive expression of RxLR23^{KM} binds to NbERD15La, impairing the binding intensity of NbERD15La and NbNAC68, which enhances the activity of NbNAC68 and activates SA defense response and inhibits the progress of infection.

Methods

Plant materials, bacterial growth conditions, and *P. capsici* culture

A pepper cultivar (*Capsicum annuum* inbred line 06221) and *Nicotiana benthamiana* were grown in controlled conditions at 25 °C with 55% humidity under 12-h light/dark cycles. Approximately 4-week-old *N. benthamiana* and 6-week-old *C. annuum* were used in this experiment. *Escherichia coli* DH5α was incubated in a Luria-Bertani medium at 37 °C. *Agrobacterium tumefaciens* GV3101 was cultivated at 28 °C in a Luria-Bertani medium. *P. capsici* (SD33, YN07, Aug0202)[75] and LT1534 strains (Supplementary Table 1) were cultured in 10% V8-juice agar at 25 °C. Zoospores were prepared for infiltration into leaves as previously described[106].

RNA extraction and qRT-PCR

To evaluate transcript levels of *RxLR23* at the early stages of *C. annuum* leaves infection with *P. capsici* SD33, each leaf was inoculated with 2.0 μL of zoospore suspension (1×10^5 zoospores/mL) and then kept at 25 °C under dark conditions. Inoculation sites were excised at 1.5, 3, 6, 12, 24, 48, and 72 hpi, and immediately dropped into liquid nitrogen. Total RNA was extracted from ground-frozen powders of mycelia (MY), sporangia (SP), zoospores (ZO), germinating cysts (GC), and different lesion samples using FastPure Universal Plant Total RNA Isolation Kit (Vazyme Biotech Co., Ltd) following the recommended protocol. Primers for qRT-PCR were designed using Primer Express 3.0 software in JGI (http://www.jgi.doe.gov/) (Supplementary Table 2). To normalize the *RxLR23* expression levels, *Pcβ*-actin, *Pcβ*-tubulin and *PcWS21* of *P. capsici*[107] were used as constitutively expressed endogenous controls. At the same time, the expression levels of *RxLR23* in mycelia was assigned to value 1.0. Transcript levels of *RxLR23* were determined in four asexual development stages of *P. capsici* or leaf lesions using qRT-PCR. Real-time quantitative PCR assay was performed using 2×SYBR Green qPCR Mix according to the manufacturer's instructions (Shandong Sparkjade Biotechnology Co., Ltd). PCR parameters were adjusted slightly as previous descriptions[106]. The

transcript levels were determined referring to the function ΔCT = CT (test gene)-CT (reference genes). The values of the threshold cycles (CT) were calculated automatically by the instrument, and the fold changes of *RxLR23* were calculated using the equation $2^{-\triangle\triangle CT}$ as previous descriptions[108]. Error bars represent standard errors calculated using three biological replicates for each sample.

CRISPR/Cas9 mediated *RxLR23* knockout in *P. capsici* strain

*RxLR23*was knocked out using CRISPR/Cas9 in *P. capsici* strain SD33 as previously described[78]. To obtained *RxLR23* mutants, the left arm and right arm sequences of *RxLR23* were edited on the cloning sequences from SD33 strain genome. *RxLR23* sgRNAs were designed using a web tool (http://grna.ctegd.uga.edu/). Low-ratio off-target sgRNAs were identified using FungiDB (https://fungidb.org/fungidb/). Secondary structures of candidate sgRNAs were further analyzed using a web tool (http://rna.urmc.rochester.edu/RNAstructureWeb/Servers/Predict1/Predict1.html). Selected sgRNAs were fused into pYF2.3G-Ribo-sgRNA. 1 kb of homology arms from both upstream and downstream of *RxLR23* were amplified and then cloned into pBluescript SK II+ along with mRFP. pYF2.3G-Ribo-sgRNA, pYF2-PsNLS-hSpCas9, and pBluescript SK II+ were finally co-transfected into *P. capsici* protoplasts to generate primary transformations. The transformants were selected on G418 resistance, followed by genomic cDNA RT-PCR. PCR amplification of the transformants and sequencing analysis were performed as described above. A 257 bp fragment of mRFP was used as a probe for Southern blots using the DIG DNA Labeling and Detection Kit (Roche). The colonies diameter of *RxLR23* mutants, unknocked strain (CK), and SD33 strain (WT) were measured, and colonies of them were imaged after 6–7 days of culture. The sporangial morphology and size of *RxLR23* mutants, CK, and WT strains were measured as previously described[106]. The number of zoospores releasing from each strain were examined as previous descriptions[109,110]. The number of releasing zoospores from single sporangium was calculated and imaged referring to previously described[111]. To estimate the virulence of mutants, 3–4 *N. benthamiana* leaves or 3–4 *C. annuum* leaves were respectively inoculated with mutants, CK and WT. The lesion leaves were imaged at 48 hpi. To examine biomass of mutants, CK, and WY strains, the lesion samples were harvested at 2 dpi, and the DNA of them was extracted as above description. To exact determine the relative biomass of *P. capsici* in *N. benthamiana* or *C. annuum* by qPCR, *Pcβ*-actin, *Pcβ-Tubulin* and *PcWS21* of *P. capsici*[33,112,113], *Caβ-actin*, *Caα-Tub*, *Caβ-Tub*, *CaEIF5A2*, *CaGAPDH*, *CaUBI-1*, *CaUBI-3*, and *Ca18S* of *C. annuum*[114], and *Nbβ-Actin*, *NbEF1α*, *NbL23*, and *NbFBOX* of *N. benthamiana*[115] were used as constitutively expressed endogenous controls, respectively. As a result, *Pcβ-actin, CaEIF5A2*, and *NbEF1α* were identified as the most suitable reference genes for the normalization of qPCR. PCR was performed on an ABI Prism 7500 Fast Real-Time PCR system (Applied Biosystems, Foster City, CA, USA). The degree of inoculation with WT was assigned to value 1.0. The relative biomass of mutants and CK strains was related to WT using ABI SDS Software V1.4. The primers used in this experiment were listed in Supplementary Table 2. Each sample was evaluated with three replicate PCR experiments.

DNA constructs

P.capsici strains (SD33, YN07, and Aug0202) and primers are listed in Supplementary Tables 1 and 2, respectively. *P. capsici* strains DNA was extracted from mycelia as previously described[106]. A putative effector RxLR23 was cloned and identified from all tested *P. capsici* strains. INF1 was cloned from *P. infestans* 88069 strain as previously described[79]. N-terminal signal peptide of RxLR23 was deleted, and a nucleotide sequence of NLS[116] or NES[117] was added to N-terminus. Full-length of CaERD15La/b/c and CaPABP were cloned from *C. annuum* cDNAs using gene-specific primers. Full-length of NbERD15La/b/c, NbNAC68a/b/c, and the promoter of *PR1/2* were respectively cloned from *N. benthamiana* cDNAs using gene-specific primers. The PCR and sequencing of them were carried out as previously described[49,53]. Allelic variants, including $RxLR23^{K93R}$, $RxLR23^{M320R}$, and $RxLR23^{K93RM320R}$, were generated using Fast Site Mutagenesis Kit referring to the Manufacturer's instructions (TIANGEN BIOTECH (BEIJING) Co., LTD). To generate pBinGFP2:$RxLR23^{KM}$, pBinGFP2:$RxLR23^{RM}$, pBinGFP2:$RxLR23^{RR}$, pBinGFP2:$RxLR23^{K93R}$, pBinGFP2:$RxLR23^{M320R}$, pBinGFP2:$RxLR23^{K93RM320R}$, pBinGFP2:$_{NLS}$RxLR23, pBinGFP2:$_{NES}$RxLR23, and pBinGFP2:INF1 (Supplementary Table 3), the PCR product of them was purified and inserted into pBinGFP2 alone. pGADT7:CaERD15La/b/c, pGADT7:CaPABP, pCHF3301-3XFLAG:CaPABP, and pCHF3301-3XFLAG:CaERD15La/b/c (Supplementary Table 3) were generated by cloning PCR product from *C. annuum* cDNA into pGADT7 and pCHF3301-3XFLAG alone using T4 DNA ligase (ACCURATE BIOTECHNOLOGY(HUNAN) CO., LTD, Chang-Sha, China). pBinGFP2:NbERD15La/b/c and pBinGFP2:NbNAC68a/b/c, pGADT7:NbERD15La/b/c, pCHF3301-3XFLAG:NbERD15La, pCHF3301-3XFLAG:NbNAC68a/b/c, pSPYCE:NbERD15La, pBI121-mCherry:Nb-NAC68a/b/c, pCAIMBIA1300-nLuc:NbERD15La, pCAIMBIA1300-cLuc:NbNAC68a/b/c, pGreenII62-SK:NbERD15La, pGreenII 62-SK:NbNAC68a/b/c, pGreenII 0800-Luc:*PR1*, and pGreenII 0800-Luc:*PR2* (Supplementary Table 3) were generated by cloning PCR product from *N. benthamiana* cDNA into pBinGFP2, pGADT7, pCHF3301-3XFLAG, pSPYCE, pBI121-mCherry, pCAIMBIA1300-nLuc, pCAIM-BIA1300-cLuc, pGreenII62-SK, and pGreenII 0800-Luc, respectively. pGBKT7:$RxLR23^{KM}$, pGBKT7:$RxLR23^{RM}$, pGBKT7:$RxLR23^{RR}$, pGBKT7:$_{NLS}$RxLR23, pGBKT7:$_{NES}$RxLR23, pSPYNE:$RxLR23^{KM}$, pCHF3301-3XFLAG:$RxLR23^{KM}$, and pCAIMBIA1300-nLuc:$RxLR23^{KM}$ (Supplementary Table 3) were generated by cloning PCR product from *P. capsici* into pGBKT7, pSPYNE, pCHF3301-3XFLAG, and pCAIMBIA1300-nLuc, respectively. To generate pSuperRFP:NbERD15La/b/c for confocal experiment, full-length of NbERD15La/b/c were cloned from *N. benthamiana* cDNA with specific primers containing the Gateway (Invitrogen) attA or attB recombination sites in the forward primer or the reverse primer, respectively. PCR products were purified and recombined into pDONR[221] (Invitrogen) to obtain entry clones through BP reactions using Gateway technology (Invitrogen). Protein fusions were prepared by recombining the entry clones with plant expression vector pSuperRFP using LR clonase (Invitrogen). All binary constructs were generated and transformed into *E. coli* DH5α and validated by sequencing using GenScript, Inc (Shanghai, China).

Agroinfiltration and gene expression

A. tumefaciens GV3101 expressing in *N. benthamiana* leaf was performed as previously described. GV3101 strains harboring the constructs were grown in liquid LB medium at 28 °C in a shaking incubator. For transient expression, each GV3101 strain was centrifuged and resuspended in agroinfiltration medium (10 mM MES, 10 mM $MgCl_2$, 150 mM acetosyringone, pH 5.6). OD_{600} was adjusted to 0.5 for transient expression of each strain. For Co-IP assay, various constructs were mixed in a 1:1 ratio to a final OD_{600} of 0.5. The cultures were then incubated for 2–3 h at 28 °C under the dark condition before infiltration. GV3101 carrying pBinGFP2:INF1 and pBinGFP2 were used as positive and negative controls, respectively. Thirty *N. benthamiana* leaves were used to assess cell death for each construct at 4 dpi. Trypan blue staining was used to quantify the degree of cell death[33].

To further evaluate whether $RxLR23^{KM}$, $RxLR23^{RM}$, and $RxLR23^{RR}$ can suppress or promote plant defense response, each infiltration site was inoculated with *P. capsici* zoospores at 24 h after agroinfiltration with each of these constructs[29]. pBinGFP2 was used as a control. Three biological replicates of each 30 *N. benthamiana* leaves were assessed. The diameter lesions were measured and photographed under UV light at 48 hpi. The relative biomass on the ratios of *P. capsici* to *N. benthamiana* leaves DNA was examined at 48 hpi using qPCR. The degree of inoculation with GFP was assigned to value 1.0. Each sample was evaluated with three replicates.

Western blot

N. benthamiana leaves by agroinfiltration of each all above constructs were harvested at 48 h. Equal amount of leaf tissues was obtained and ground in liquid nitrogen immediately. The powdered extracts mixed with SDS-loading buffer were boiled for 10 min, and the protein supernatant recovered after centrifugation at 13,000 × *g* for 10 min. Protein samples were run on 12% SDS-PAGE gels and then transferred to PVDF membrane (Merck KGaA) (pretreated with methanol for 30 s) using a transfer buffer (20 mM Tris-base, 150 mM glycine, 20% methanol) (Sigma-Aldrich). The membrane was blocked using TBST (0.15 M NaCl, 10 mM Tris-HCl pH 8.0, 0.1% Tween 20) (Sigma-Aldrich) plus 5% nonfat dry milk (Solarbio) for 2 h with gentle shaking. Mouse anti-GFP, anti-FLAG, and anti-mCherry monoclonal antibodies (ABclonal Technology (WuHan, China)), as the primary antibodies, were added to the TBST at a ratio of 1:5000. The membrane was incubated for 90 min followed by washing three times (5 min each) with TBST. The membrane was then incubated with HRP goat anti-mouse lgG (H + L) antibody (ABclonal Technology (WuHan, China)) at a ratio of 1:5000 in TBST for 50 min with gentle shaking followed by washing three times (5 min each) with TBST. Antibodies were visualized using Super ECL Detection Reagent ECL (Yeasen Biotechnology (Shanghai) Co., Ltd) and a Tanon 5200 system. The antibody of plant *β*-Tubulin (ABclonal Technology (WuHan, China)) was used as an endogenous protein for the normalization of electroblotting proteins in all lanes. Protein loading is indicated by Ponceau Staining (Ponceau S) staining. Each experiment was repeated at least three times.

Y2H

A Y2H screen with pGBKT7:RxLR23^{KM} was performed following a strategy designed to identify effector interactors. RxLR23^{KM} without the signal peptide was cloned into pGBKT7 (Takara Bio). cDNA library of *C. annuum* inbred line06221 was constructed in yeast strain Y187 using total RNA extracted from *C. annuum* leaves from 12 h to 72 h (12 h-intervals) after inoculation with *P. capsici*. The cDNA library with estimated 2×10^7 primary yeast clones was screened using pGBKT7:RxLR23^{KM} as the bait. Potential yeast transformants containing target proteins were selected using SD/-Trp/-Leu/-His/X-α-gal selective medium (TaKaRa Bio). Several target genes were identified and full-length sequences of them were cloned from *C. annuum* cDNA into pGADT7 (TaKaRa Bio) alone. Recombined pGADT7 constructs were used as the prey vectors. The bait vector pGBKT7:RxLR23^{KM} and each prey vector were co-transformed into the yeast strain Y2Hgold. Transformants, appearing on the SD/-Trp/-Leu medium (TaKaRa Bio), were isolated and detected for growth on the SD/-Trp/-Leu/-His/-Ade/X-α-gal plates (TaKaRa Bio). Each experiment was repeated at least three times.

BiFC

For BiFC assay, leaves of 4 to 5 weeks *N. benthamiana* were infiltrated with GV3101 carrying constructs harboring the N-terminus of the YFP (YFPn) fragment fused to RxLR23^{KM}, and the C-terminus of YFP (YFPc) fragment fused to the target protein. To inoculate *N. benthamiana* leaves, OD_{600} of each above cultures was adjusted to 1.0 and equal volumes were mixed. Leaf pieces were cut at 2–3 days after agroinfiltration and then placed on a sliding glass where water was dropped before adding a cover glass. Leaves were imaged using a Zeiss 710 confocal laser scanning microscope using a 514 nm laser line to excite the YFP and a spectrum of 525 to 560 nm to collect emissions. To generate high-quality images, stacked images were acquired as 1 μm planar sections and assembled using ImageJ. Each experiment was repeated at least three times.

Co-IP and LC-MS/MS analysis

Above corresponding constructs for Co-IP were transiently expressed in *N. benthamiana* leaves. Leaf samples were collected 2 days after agroinfiltration and proteins were extracted using lysis buffer (50 mM HEPES, 150 mM KCl, 1 mM EDTA, 10 mM KOH (pH 7.5), and 10% Triton X-100) (Sigma-Aldrich) with 1 M DTT, and protease inhibitor cocktail (1 μg/mL pepstatin A and 1 μg/mL leupeptin) (Sigma-Aldrich). Protein extracts were incubated with Anti-GFP (Nanobody) Agarose Beads or Affinity Gel-conjugated Mouse anti DDDDK-Tag mAb (ABclonal Technology (WuHan, China) for 4 h at 4 °C. Beads were washed three times in lysis buffer and then mixed with 2×SDS loading buffer. For Co-IP, proteins were detected by western blots. For LC-MS/MS, NbERD15La was transiently expressed in *N. benthamiana* leaves in contrast to GFP (control) ($n = 3$ independent experiments). Leaf samples were collected and extracted as above description. Protein extracts were incubated with Anti-GFP (Nanobody) Agarose Beads for 4 h at 4 °C. Beads were washed three times in lysis buffer and proteins were separated with SDS/PAGE and the gels were cut into slices (~5 × 10 mm). Proteins contained in gel slices were prepared for LC-MS/MS. In LC-MS/MS assay, the peptide samples were carried out on a Q Exactive HF-X mass spectrometer coupled with an Easy-nLC 1200 system for LC-MS/MS Detection. The LC-MS analysis was performed by SpecAllyLife Technology Co., Ltd. (Wuhan, China). Database Search MS raw data were analyzed with MaxQuant (V1.6.6) using the Andromeda database search algorithm. Proteins with a fold change >4 between bait IP and control were screened out as interactors of the bait protein.

Protein purification and microscale thermophoresis (MST)

The plasmids of HIS-Trx-labeled NbNAC68a/b/c, HIS-labeled RxLR23^{KM}, GST-labeled NbERD15La, and GST-labeled RxLR23^{KM} were obtained alone. DH5α cells (Trelief™ 5α Chemically Competent Cell, Tsingke Biological Technology) were used for cloning, and *Escherichia coli* strains BL21 (DE3) (CD601-01, TransGen Biotech) were used for protein expression following induction by isopropyl β-D-1-thiogalactopyranoside (IPTG, 1.0 mmol/L, 16 °C, 16 h). The proteins were purified with HIS-labeled or GST-labeled purification kit. Proteins with H-Trx-label were then eluted with gradient concentration imidazole (Sangon Biotech, A600277) and cleaved the Trx-label of NbNAC68a/b/c proteins using Thrombin (Sigma) that is then removed by Benzamidine Sepharose 6B (Sigma). Also, two another proteins with GST-label were eluted with L-Glutathione reduced (Sigma), followed by cleaving GST-label of NbERD15La protein and RxLR23^{KM} protein using HRV-3C (Sigma) alone. Finally, all these tested proteins were enriched by ultrafiltration (MWCO 10 kD or 30KD Millipore) and preserved in 300 mM NaCl added 30 mM HEPES or added 30 mM Tris at −80 °C.

For MST experiment, the equilibrium dissociation constant (Kd) values were measured using the Monolith NT.115 instrument (NanoTemper Technologies) referring to described previously[118]. The RxLR23^{KM}-HIS and NbNAC68a/b/c-HIS proteins were respectively fluorescently labeled according to manufacturer's protocol using HIS-tag red channel (MO-L018). NbERD15La was diluted to the needed concentration (from 125 mM to 1.9 nM) and incubated with 200 nM of fluorescently labeled NbNAC68a/b/c-HIS or RxLR23^{KM}-HIS protein for 15 min. To detect the interaction of NbERD15La with RxLR23^{KM} and NbNAC68a/b/c, 40 mM of RxLR23^{KM} protein was added into a complex mixture, containing NbNAC68a/b/c and NbERD15La. The samples were loaded into the NanoTemper glass capillaries (MO-K025) and microthermophoresis was carried out using 40% light emitting diode power. The Kd values were calculated using the mass action equation via the NanoTemper software from duplicate reads of measurements. Each experiment was repeated at least three times.

Luciferase complementation imaging assay (LCI)

For LCI assay, GV3101 harboring pCAIMBIA1300-nLuc:NbERD15La, pCAIMBIA1300-cLuc:NbNAC68a/b/c, and pCAIMBIA1300-cLuc:RxLR23^{KM} were infiltrated into *N. benthamiana* leaves alone. pCAMBIA1300-nLuc:MBP and pCAMBIA1300-cLuc:GST were used as controls. These leaves were sprayed with 1 mM D-Luciferin potassium

(Meilunbio) at 48 h after infiltration, and then kept in the dark for 5 min. The subsequent signals were immediately recorded for 20 min using with Tanon-5200 Multi-Imaging System. To calculate the luminescence intensity, leaf discs were inoculated all above constructs at 48 h and then incubated with 1 mM D-Luciferin potassium (Meilunbio) in 96-well plates for 10 min. The luminescence intensity was detected using a microplate reader. Each experiment was repeated at least three times.

Dual-luciferase reporter assay

Full-length of NbNAC68a/b/c, NbERD15La, and RxLR23^{KM} were cloned into pGreenII62-SK alone, and *PR1/2* promoter was cloned into pGreenII0800-Luc respectively. The *PR1/2* promoter-driven luciferase gene was delivered by GV3101 harboring pSoup-P19 into *N. benthamiana* leaves that mixed with RxLR23^{KM}, NbNAC68a/b/c, NbERD15La, NbERD15La + NbNAC68a/b/c, NbERD15La + NbNAC68a/b/c + RxLR23^{KM}, and pGreenII62-SK (control), respectively. After 48 h, *N. benthamiana* leaves were treated referring to described under luciferase complementation imaging to acquire chemiluminescence images. Leaf samples were collected for the dual-Luc using commercial dual-Luc reaction reagents (Meilunbio). Leaves were grounded in liquid nitrogen and homogenized in 100 ml of Cell Lysis buffer (Meilunbio). Crude extract (8 mL) was mixed with 40 mL of Luciferase buffer (Meilunbio), and firefly luciferase activity was measured. Subsequently, 40 mL Stop and Glow buffer (Meilunbio) was added to quench the firefly luciferase and to initiate the REN luciferase reaction. Three biological repeats were measured for each sample.

Electrophoretic mobility shift assay (EMSA)

Production and purification of NbNAC68a/b/c, NbERD15La or RxLR23^{KM} proteins were used as EMSA assay[119]. EMSA was performed using the Chemiluminescent EMSA Kit (#GS009; Beyotime) referring to the manufacturer's protocol. Complementary pairs of 3'-end biotin labeled and unlabeled oligonucleotides of NbNAC68a/b/c recognition sites (PR1-F: ATTTCATGACACGTATCCAACTTAAAC, PR1-R: GTTTAAGTTGGATACGTGTCATGAAAT; PR2-F: GTATCAAATACACGTAAATGAGTTGTTG, PR2-R: CAACAACTCATTTACGTGTATTTGATAC) were annealed using EMSA Probe Biotin Labeling Kit (#GS008; Beyotime) and used as probes for EMSA studies. The protein-DNA samples were then separated on 6% polyacrylamide gels and signals were captured with Tanon-5200 Multi-Imaging System. Each experiment was repeated at least three times.

Confocal microscopy

Agrobacterium GV3101 strains carrying above corresponding constructs were individually infiltrated into the 4-week-old *N. benthamiana* leaves after being adjusted to a final OD_{600} of 0.5. The epidermal cells of *N. benthamiana* were imaged at 2–3 d using Zeiss 710 confocal microscope. The GFP was excited with 488 nm from an argon laser and detected at 500 to 530 nm. The RFP/mCherry was excited with 561 nm from a diode laser and detected at 600 to 630 nm. The GFP and RFP/mCherry were used as controls. The pinhole was set at 1 airy unit for the longest light wavelength emission. In these experiments, we discovered localizations of RxLR23^{KM} and its isoforms, $_{NES}$RxLR23, and $_{NLS}$RxLR23, and the co-localizations of RxLR23^{KM} with NbERD15La/b/c, NbERD15La with NbNAC68a/b/c, and NbERD15La with NbNAC68a/b/c under RxLR23-FLAG treatment. The variation of RxLR23^{KM} and its isoforms expression was measured upon the ratio of nucleolar to nucleoplasm with fluorescence intensity. The brightest segments with the nucleolus in optical sections were collected, and the mean intensities of fluorescence were measured in the nucleoplasm and the nucleolus separately after drawing regions of interest to encompass them. Images were processed using the Zeiss 710 LSM, ImageJ, and Adobe Photoshop software packages. These experiments were repeated at least three times.

ERD15 and ERD15L sequences analysis

NbERD15La/b/c were downloaded from Sol Genomics Network (https://solgenomics.net/). All other ERD15 and ERD15L sequences were downloaded from NCBI (https://www.ncbi.nlm.nih.gov/) (Supplementary Table 4). All these ERD15L and ERD15 sequences were aligned using ClustalX 2.0[120]. Phylogenetic trees were generated by neighbor-joining using PAUP*4.0 Beta with the default parameters. Nodal support of the trees was estimated by bootstrapping with 1000 pseudoreplicate data sets. The protein conserved domains were predicted on the website (https://www.ncbi.nlm.nih.gov/Structure/cdd/wrpsb.cgi).

Arabidopsis thaliana transformation and selection transgenic plants

pBinGFP2:RxLR23^{KM}, pBinGFP2:RxLR23^{RM}, pBinGFP2:RxLR23^{RR}, and pBinGFP2 were respectively transformed into 5-week-old *A. thaliana* (Col-0) plants with several mature flowers via *A. tumefaciens* GV3101 by method of floral dip[121]. *A. thaliana* (Col-0) (WT) and pBinGFP2 (CK) were used as controls. The seedlings of transgenic *A. thaliana* were selected by growing surface-sterilized T1 seeds on 1/2MS plates containing 50 μg mL^{-1} kanamycin and 10-day-old transgenic seedlings were then transferred into soil pots. Phenotypes of these transgenic plants were observed T1 generation following the T2 or T3 generation. RT-PCR was used to measure these genes in transgenic plants. Expression of RxLR23^{KM}, RxLR23^{RM}, and RxLR23^{RR} in T2 or T3 transgenic plants was detected by western blots using GFP-antibodies. Six transgenic lines with similar phenotypes were obtained.

VIGS

In our experiments, the amplicons were characteristically suitable for silencing NbERD15La or/and NbNAC68a/b/c sequences. VIGS constructs were generated by cloning a specific 300 bp fragment of NbERD15La, NbERD15Lb, NbERD15Lc or NbNAC68a/b/c from *N. benthamiana* cDNA into the binary vector TRV2 using the restriction sites to obtain TRV2:NbERD15La, TRV2:NbERD15Lb, TRV2:NbERD15Lc, or TRV2:NbNAC68a/b/c (Supplementary Table 3)[122]. Also, VIGS constructs were generated by cloning a 400 bp fragment containing 200 bp of NbERD15La and 200 bp of NbNAC68a/b/c from *N. benthamiana* cDNA into the binary vector TRV2 using the restriction sites to obtain TRV2:NbERD15La-NbNAC68a/b/c (Supplementary Table 3). Briefly, *Agrobacterium* GV3101 strains harboring a mixture of TRV1 and TRV2:GFP, and a mixture of TRV1 and TRV2:NbERD15La, TRV2:NbERD15Lb, TRV2:NbERD15Lc, TRV2:NbNAC68a/b/c, or TRV2:NbERD15La-NbNAC68a/b/c in a 1:1 ratio to achieve OD_{600} of 0.5 each. The mixture of TRV1 and TRV2:GFP or TRV1 and TRV2:PDS was used as a negative or positive control. The two largest leaves of five-leaf-stage *N. benthamiana* were infiltrated with each of the mixtures in each plant. However, expression levels of *NbERD15La* or *NbNAC68a/b/c* were detected in silenced plants by qRT-PCR at 3 to 4 weeks after inoculation, respectively. *NbEF1α* of *N. benthamiana* were used as a constitutively expressed endogenous control to normalize the expression of *NbERD15La/b/c* or NbNAC68a/b/c. To avoid the ectopically expressed genes were silenced in TRV plants, we generated a synthetic version of NbERD15La and GFP with shuffled synonymous codon sequences. Three biological replicates of each 15 leaves were assessed for each construct. Either *t* test or one-way ANOVA and Tukey Honest Significant Difference Tests were performed for statistical analysis. Each experiment was repeated at least three times.

Trypan blue and DAB staining

Cell death in *N. benthamiana* and *C. annuum* leaves was examined using trypan blue staining. Agroinfiltrated leaves were harvested at 48 hpi and soaked in boiling trypan blue solution (10 mL lactic acid, 10 mL glycerol, 10 mL distilled water, 10 g phenol, and 0.02 g trypan blue) (Sigma-Aldrich) for 1.5 min or 2.0 min of *N. benthamiana* and *C.*

annuum leaves respectively, and then incubated for 12 h. Samples were decolorized in 9 mol/L chloral hydrate solution (Sigma-Aldrich) for 5 days (1 day intervals) and then soaked in 95% ethanol (Sigma-Aldrich) for 5–6 h to further remove the background. Images were photographed under natural light. These experiments were independently repeated at least three times.

H_2O_2 accumulation in inoculation sites of *N. benthamiana* leaves was visualized by staining with 3, 3′-diaminobenzidine (DAB) (Sigma-Aldrich). Agroinfiltrated leaves were detached at 36 h after inoculation and then soaked in DAB solution (1 mg/mL; Horseradish Catalase DAB Color Kit) (Sangon Biotech, China) and maintained at 28 °C for 12 h. Leaf samples were finally discolored in a destaining solution (150 mL ethanol, 10 mL glycerol, and 40 mL distilled water) under 65 °C for 72 h (24 h-intervals). Images were photographed under natural light. These experiments were independently repeated at least three times.

Electrolyte leakage

Agroinfiltrated leaves were harvested and washed twice with sterile water at 48 h before being used to prepare leaf discs with a diameter of 9 mm. Leaf discs were first soaked in 15 mL deionized water (15 discs per sample, three samples per biological replicate). After shaking for 3 h at room temperature, the conductivity of different samples was measured individually using a conductivity meter (METTLER TOLEDO) and the values were recorded as A. Subsequently, samples were boiled for 25 min and naturally cooled to room temperature. The conductivity was measured as B, which represented the total conductivity. The ion leakage was calculated as A/B ratio and the mean was used for final analysis.

SA measurement

Agrobacterium strains harboring pBinGFP2:RxLR23^{KM}, pBinGFP2:NbNAC68a, pBinGFP2:NbERD15La, and pBinGFP2 were ectopically expressed in *N. benthamiana* leaves, respectively. The procedures for SA extraction and measurement were referred to in previous descriptions[123]. Approximately 100 mg of each infiltrated leaf was excised at 12, 24, 36, 48, and 60 h and immediately ground in liquid nitrogen. Each sample was added 0.6 mL of 90% methanol, and vortexed for 20 s and then sonicated for 20 min to release SA. Samples were then centrifuged at 12,000 × *g* for 10 min under 4 °C. The supernatant was collected and added 0.5 mL of 100% methanol to the pellet for the second round of extraction. The supernatant from these two extractions was combined and dried by vacuum. For free-SA measurement, 0.5 ml 5% (w/v) trichloroacetic acid was added to the dry samples following vortexed and sonicated for 5 min. The samples were subsequently centrifuged at 12,000 × *g* for 15 min at 4 °C. The supernatant was collected and extracted three times with 0.5 mL extraction buffer (ethylacetate acid/cyclopentane/isopropanol at 100:99:1 by volume). Each time, the organic phase was collected and combined into a new tube and dried by vacuum after centrifugation at 12,000 × *g* for 10 min at 4 °C. The final dried samples were resuspended in 200 µl mobile phase (0.2 M KAc, 0.5 mM EDTA pH 5) by vortexing and sonication for 5 min. After spinning at 12,000 × *g* for 5 min at 4 °C, the supernatant was kept and analyzed by high performance liquid chromatography-mass spectrometry (HPLC-MS) to measure the amount of SA compared with a standard. Three biological repeats were used in each experiment.

ABA measurement

The procedures for ABA extraction and measurement referred to in previous descriptions[123]. Each infiltrated leaf for ABA measurement were also excised at 12, 24, 36, 48, and 60 h and immediately ground in liquid nitrogen. Each sample was extracted from 100 mg of frozen ground leaves with 0.6 mL of 90% methanol. The extracts were then subjected to ultrasonication and vortexing for 30 min. Samples were centrifuged at 13,000 × *g* for 10 min at 4 °C. The supernatants were collected and re-extracted with 0.5 mL of 100% methanol, and finally filtered with a C18 solid phase extraction column (Agilent SampliQ C18 SPE, 3 µm) before analysis. Samples were analyzed by HPLC-MS as previously reported[124]. Quantification of ABA was made upon the recovery rates of each sample compared with a standard. Three biological repeats were used in each experiment.

Statistics and reproducibility

The data graphs were drawn using GraphPad Prism (8.0.1). No data were excluded from the study. Randomization and blinding were used in the study. The data were subjected to a one-way analysis of variance (ANOVA). Student's *t* test was used for two means, and Duncan's multiple range test of least significant difference (LSD) was used for more than two means. *p* values of 0.05, 0.01, or 0.001 were used as indicated.

Reporting summary

Further information on research design is available in the Nature Portfolio Reporting Summary linked to this article.

Data availability

The authors declare that all data supporting the findings of this study are available within the manuscript and the Supplementary Files are available from the corresponding authors upon request. The proteomics data were deposited to the ProteomeXchange Consortium via the iProX partner repository with the dataset identifier PXD046771. Source data are provided with this paper.

References

1. Wu, C. H., Derevnina, L. & Kamoun, S. Receptor networks underpin plant immunity. *Science* **360**, 1300–1301 (2018).
2. Yan, Q., Rogan, C. J. & Anderson, J. C. Development of a *Pseudomonas syringae-Arabidopsis* suspension cell infection system for investigating host metabolite-dependent regulation of type III secretion and pattern-triggered immunity. *Mol. Plant Microbe Interact.* **32**, 527–539 (2019).
3. Gallun, R. L., Starks, K. J. & Guthrie, W. D. Plant resistance to insects attacking cereals. *Annu. Rev. Entomol.* **20**, 337–357 (1975).
4. Asai, S., Ohta, K. & Yoshioka, H. MAPK signaling regulates nitric oxide and NADPH oxidase-dependent oxidative bursts in *Nicotiana benthamiana*. *Plant Cell* **20**, 1390–1406 (2008).
5. Adachi, H. et al. WRKY transcription factors phosphorylated by MAPK regulate a plant immune NADPH oxidase in *Nicotiana benthamiana*. *Plant Cell* **27**, 2645–2663 (2015).
6. Block, A. et al. The *Pseudomonas syringae* type III effector HopG1 targets mitochondria, alters plant development and suppresses plant innate immunity. *Cell Microbiol.* **12**, 318–330 (2010).
7. Krasileva, K. V., Dahlbeck, D. & Staskawicz, B. J. Activation of an *Arabidopsis* resistance protein is specified by the in planta association of its leucine-rich repeat domain with the cognate oomycete effector. *Plant Cell* **22**, 2444–2458 (2010).
8. Wang, W., Liu, N., Gao, C., Rui, L. & Tang, D. The *Pseudomonas Syringae* effector AvrPtoB associates with and ubiquitinates *Arabidopsis* exocyst subunit EXO70B1. *Front. Plant Sci.* **10**, 1027 (2019).
9. Jones, J. D. & Dangl, J. L. The plant immune system. *Nature* **444**, 323–329 (2006).
10. Birch, P. R., Rehmany, A. P., Pritchard, L., Kamoun, S. & Beynon, J. L. Trafficking arms: oomycete effectors enter host plant cells. *Trends Microbiol.* **14**, 8–11 (2006).
11. Kamoun, S. A catalogue of the effector secretome of plant pathogenic oomycetes. *Annu. Rev. Phytopathol.* **44**, 41–60 (2006).
12. Mccarthy, C. G. & Fitzpatrick, D. A. Phylogenomic reconstruction of the oomycete phylogeny derived from 37 genomes. *mSphere* **2**, e00095–17 (2017).

13. Baxter, L. et al. Signatures of adaptation to obligate biotrophy in the *Hyaloperonospora arabidopsidis* genome. *Science* **330**, 1549–1551 (2010).
14. Haas, B. J. et al. Genome sequence and analysis of the Irish potato famine pathogen *Phytophthora infestans*. *Nature* **461**, 393–398 (2009).
15. Jiang, R. H. et al. RXLR effector reservoir in two *Phytophthora* species is dominated by a single rapidly evolving superfamily with more than 700 members. *Proc. Natl Acad. Sci. USA* **105**, 4874–4879 (2008).
16. Tyler, B. M. et al. *Phytophthora* genome sequences uncover evolutionary origins and mechanisms of pathogenesis. *Science* **313**, 1261–1266 (2006).
17. Shi, J. et al. Improved whole-genome sequence of *Phytophthora capsici* generated by long-read sequencing. *Mol. Plant Microbe Interact.* **34**, 866–869 (2021).
18. Stajich, J. E. et al. High-quality reference genome sequence for the oomycete vegetable pathogen *Phytophthora capsici* strain LT1534. *Microbiol. Resour. Announc.* **10**, e0029521 (2021).
19. Lamour, K. H., Stam, R., Jupe, J. & Huitema, E. The oomycete broad-host-range pathogen *Phytophthora capsici*. *Mol. Plant Pathol.* **13**, 329–337 (2012).
20. Whisson, S. C. et al. A translocation signal for delivery of oomycete effector proteins into host plant cells. *Nature* **450**, 115–118 (2007).
21. Dou, D. et al. RXLR-mediated entry of *Phytophthora sojae* effector Avr1b into soybean cells does not require pathogen-encoded machinery. *Plant Cell* **20**, 1930–1947 (2008).
22. Whisson, S. C., Boevink, P. C., Wang, S. & Birch, P. R. The cell biology of late blight disease. *Curr. Opin. Microbiol.* **34**, 127–135 (2016).
23. Jing, M. et al. A *Phytophthora sojae* effector suppresses endoplasmic reticulum stress-mediated immunity by stabilizing plant binding immunoglobulin proteins. *Nat. Commun.* **7**, 11685 (2016).
24. Kong, G. et al. The activation of *Phytophthora* effector Avr3b by plant cyclophilin is required for the nudix hydrolase activity of Avr3b. *PLoS Pathog.* **11**, e1005139 (2015).
25. Anderson, R. G., Deb, D., Fedkenheuer, K. & Mcdowell, J. M. Recent progress in RXLR effector research. *Mol. Plant Microbe Interact.* **28**, 1063–1072 (2015).
26. Engelhardt, S. et al. Relocalization of late blight resistance protein R3a to endosomal compartments is associated with effector recognition and required for the immune response. *Plant Cell* **24**, 5142–5158 (2012).
27. Oh, S. K. et al. In planta expression screens of *Phytophthora infestans* RXLR effectors reveal diverse phenotypes, including activation of the *Solanum bulbocastanum* disease resistance protein Rpi-blb2. *Plant Cell* **21**, 2928–2947 (2009).
28. Saunders, D. G. et al. Host protein BSL1 associates with *Phytophthora infestans* RXLR effector AVR2 and the *Solanum demissum* immune receptor R2 to mediate disease resistance. *Plant Cell* **24**, 3420–3434 (2012).
29. Bos, J. I. et al. *Phytophthora infestans* effector AVR3a is essential for virulence and manipulates plant immunity by stabilizing host E3 ligase CMPG1. *Proc. Natl Acad. Sci. USA* **107**, 9909–9914 (2010).
30. Gilroy, E. M. et al. CMPG1-dependent cell death follows perception of diverse pathogen elicitors at the host plasma membrane and is suppressed by *Phytophthora infestans* RXLR effector AVR3a. *N. Phytol.* **190**, 653–666 (2011).
31. Yang, L. et al. Potato NPH3/RPT2-like protein StNRL1, targeted by a *Phytophthora infestans* RXLR effector, is a susceptibility factor. *Plant Physiol.* **171**, 645–657 (2016).
32. He, Q. et al. Plant pathogen effector utilizes host susceptibility factor NRL1 to degrade the immune regulator SWAP70. *Proc. Natl Acad. Sci. USA* **115**, 7834–7843 (2018).
33. Li, Q. et al. A *Phytophthora capsici* effector targets ACD11 binding partners that regulate ROS-mediated defense response in *Arabidopsis*. *Mol. Plant* **12**, 565–581 (2019).
34. Xiong, Q. et al. *Phytophthora* suppressor of RNA silencing 2 is a conserved RxLR effector that promotes infection in soybean and *Arabidopsis thaliana*. *Mol. Plant Microbe Interact.* **27**, 1379–1389 (2014).
35. Hou, Y. et al. A *Phytophthora* effector suppresses trans-kingdom RNAi to promote disease susceptibility. *Cell Host Microbe* **25**, 153–165.e155 (2019).
36. Yin, X. et al. An RxLR effector from *Plasmopara viticola* suppresses plant immunity in grapevine by targeting and stabilizing VpBPA1. *Plant J.* **112**, 104–114 (2022).
37. Huang, G. et al. An RXLR effector secreted by *Phytophthora parasitica* is a virulence factor and triggers cell death in various plants. *Mol. Plant Pathol.* **20**, 356–371 (2019).
38. Liu, J. et al. *Plasmopara viticola* effector PvRXLR53 suppresses innate immunity in *Nicotiana benthamiana*. *Plant Signal. Behav.* **16**, 1846927 (2021).
39. Qi, G. et al. Pandemonium breaks out: disruption of salicylic acid-mediated defense by plant pathogens. *Mol. Plant* **11**, 1427–1439 (2018).
40. Caillaud, M. C. et al. A downy mildew effector attenuates salicylic acid-triggered immunity in *Arabidopsis* by interacting with the host mediator complex. *PLoS Biol.* **11**, e1001732 (2013).
41. Liu, T. et al. Unconventionally secreted effectors of two filamentous pathogens target plant salicylate biosynthesis. *Nat. Commun.* **5**, 4686 (2014).
42. Situ, J. et al. Oomycete pathogen pectin acetylesterase targets host lipid transfer protein to reduce salicylic acid signaling. *Plant Physiol.* https://doi.org/10.1093/plphys/kiad638 (2023).
43. Nomura, K. et al. A bacterial virulence protein suppresses host innate immunity to cause plant disease. *Science* **313**, 220–223 (2006).
44. Wirthmueller, L. et al. *Arabidopsis* downy mildew effector HaRxL106 suppresses plant immunity by binding to RADICAL-INDUCED CELL DEATH1. *N. Phytol.* **220**, 232–248 (2018).
45. Sharpee, W. C. & Dean, R. A. Form and function of fungal and oomycete effectors. *Fungal Biol. Rev.* **30**, 62–73 (2016).
46. Wang, Q. et al. Transcriptional programming and functional interactions within the *Phytophthora sojae* RXLR effector repertoire. *Plant Cell* **23**, 2064–2086 (2011).
47. Zheng, X. et al. Functionally redundant RXLR effectors from *Phytophthora infestans* act at different steps to suppress early flg22-triggered immunity. *PLoS Pathog.* **10**, e1004057 (2014).
48. Kiyosue, T., Yamaguchi-Shinozaki, K. & Shinozaki, K. ERD15, a cDNA for a dehydration-induced gene from *Arabidopsis thaliana*. *Plant Physiol.* **106**, 1707 (1994).
49. Alves, M. S. et al. A novel transcription factor, ERD15 (Early Responsive to Dehydration 15), connects endoplasmic reticulum stress with an osmotic stress-induced cell death signal. *J. Biol. Chem.* **286**, 20020–20030 (2011).
50. Alves, M. S., Fontes, E. P. & Fietto, L. G. EARLY RESPONSIVE to DEHYDRATION 15, a new transcription factor that integrates stress signaling pathways. *Plant Signal. Behav.* **6**, 1993–1996 (2011).
51. Kariola, T. et al. EARLY RESPONSIVE TO DEHYDRATION 15, a negative regulator of abscisic acid responses in *Arabidopsis*. *Plant Physiol.* **142**, 1559–1573 (2006).
52. Timmusk, S. & Wagner, E. G. The plant-growth-promoting rhizobacterium *Paenibacillus polymyxa* induces changes in *Arabidopsis thaliana* gene expression: a possible connection between biotic and abiotic stress responses. *Mol. Plant Microbe Interact.* **12**, 951–959 (1999).

53. Olsen, A. N., Ernst, H. A., Leggio, L. L. & Skriver, K. NAC transcription factors: structurally distinct, functionally diverse. *Trends Plant Sci.* **10**, 79–87 (2005).
54. Zhong, R., Lee, C. & Ye, Z. H. Functional characterization of poplar wood-associated NAC domain transcription factors. *Plant Physiol.* **152**, 1044–1055 (2010).
55. Kim, H. J., Nam, H. G. & Lim, P. O. Regulatory network of NAC transcription factors in leaf senescence. *Curr. Opin. Plant Biol.* **33**, 48–56 (2016).
56. Puranik, S., Sahu, P. P., Srivastava, P. S. & Prasad, M. NAC proteins: regulation and role in stress tolerance. *Trends Plant Sci.* **17**, 369–381 (2012).
57. Christianson, J. A., Dennis, E. S., Llewellyn, D. J. & Wilson, I. W. ATAF NAC transcription factors: regulators of plant stress signaling. *Plant Signal. Behav.* **5**, 428–432 (2010).
58. Nuruzzaman, M., Sharoni, A. M. & Kikuchi, S. Roles of NAC transcription factors in the regulation of biotic and abiotic stress responses in plants. *Front. Microbiol.* **4**, 248 (2013).
59. Yoshii, M. et al. Disruption of a novel gene for a NAC-domain protein in rice confers resistance to rice dwarf virus. *Plant J.* **57**, 615–625 (2009).
60. Huang, Y., Li, T., Xu, Z. S., Wang, F. & Xiong, A. S. Six NAC transcription factors involved in response to TYLCV infection in resistant and susceptible tomato cultivars. *Plant Physiol. Biochem.* **120**, 61–74 (2017).
61. Wang, F. T. et al. TaNAC1 acts as a negative regulator of stripe rust resistance in wheat, enhances susceptibility to *Pseudomonas syringae*, and promotes lateral root development in transgenic *Arabidopsis thaliana*. *Front. Plant Sci.* **6**, 108 (2015).
62. Chang, Y. et al. NAC transcription factor involves in regulating bacterial wilt resistance in potato. *Funct. Plant Biol.* **47**, 925–936 (2020).
63. Sun, L. et al. Functions of rice NAC transcriptional factors, ONAC122 and ONAC131, in defense responses against *Magnaporthe oryzae*. *Plant Mol. Biol.* **81**, 41–56 (2013).
64. Liu, Q. et al. NAC transcription factor OsNAC066 positively regulates disease resistance by suppressing the ABA signaling pathway in rice. *Plant Mol. Biol.* **98**, 289–302 (2018).
65. Wang, Z. et al. Osa-miR164a targets OsNAC60 and negatively regulates rice immunity against the blast fungus *Magnaporthe oryzae*. *Plant J.* **95**, 584–597 (2018).
66. Zhang, X. M. et al. TaNAC2 is a negative regulator in the wheat-stripe rust fungus interaction at the early stage. *Physiol. Mol. Plant Pathol.* **102**, 144–153 (2018).
67. Wang, B. et al. A novel wheat NAC transcription factor, TaNAC30, negatively regulates resistance of wheat to stripe rust. *J. Integr. Plant Biol.* **60**, 432–443 (2018).
68. Zhou, W. H. et al. TaNAC6s are involved in the basal and broad-spectrum resistance to powdery mildew in wheat. *Plant Sci.* **277**, 218–228 (2018).
69. Perochon, A. et al. A wheat NAC interacts with an orphan protein and enhances resistance to *Fusarium* head blight disease. *Plant Biotechnol. J.* **17**, 1892–1904 (2019).
70. Xia, N. et al. TaNAC8, a novel NAC transcription factor gene in wheat, responds to stripe rust pathogen infection and abiotic stresses. *Physiol. Mol. Plant Pathol.* **74**, 394–402 (2010).
71. Meisrimler, C. N., Pelgrom, A. J. E., Oud, B., Out, S. & den Ackerveken, G. V. Multiple downy mildew effectors target the stress-related NAC transcription factor LsNAC069 in lettuce. *Plant J.* **99**, 1098–1115 (2019).
72. Shapiguzov, A. et al. *Arabidopsis* RCD1 coordinates chloroplast and mitochondrial functions through interaction with ANAC transcription factors. *eLife* **8**, e43284 (2019).
73. McLellan, H. et al. An RxLR effector from *Phytophthora infestans* prevents re-localisation of two plant NAC transcription factors from the endoplasmic reticulum to the nucleus. *PLoS Pathog.* **9**, e1003670 (2013).
74. Erwin, D. C. & Ribeiro, O. K. *Phytophthora* Diseases Worldwide (The American Phytopathological Society, 1996).
75. Sun, W. X., Jia, Y. J., O'Neill, N. R., Feng, B. Z. & Zhang, X. G. Genetic diversity in *Phytophthora capsici* from eastern China. *Can. J. Plant Pathol.* **30**, 414–424 (2008).
76. Chen, X. R. et al. The RXLR effector PcAvh1 is required for full virulence of *Phytophthora capsici*. *Mol. Plant Microbe Interact.* **32**, 986–1000 (2019).
77. Song, T. et al. An oomycete CRN effector reprograms expression of plant HSP genes by targeting their promoters. *PLoS Pathog.* **11**, e1005348 (2015).
78. Fang, Y., Cui, L., Gu, B., Arredondo, F. & Tyler, B. M. Efficient genome editing in the oomycete *Phytophthora sojae* using CRISPR/Cas9. *Curr. Protoc. Microbiol.* **44**, 21A.1.1–21A.1.26 (2017).
79. Kamoun, S., van West, P., Vleeshouwers, V. G., de Groot, K. E. & Govers, F. Resistance of *Nicotiana benthamiana* to *Phytophthora infestans* is mediated by the recognition of the elicitor protein INF1. *Plant Cell* **10**, 1413–1426 (1998).
80. Boevink, P. et al. A *Phytophthora infestans* RXLR effector targets plant PP1c isoforms that promote late blight disease. *Nat. Commun.* **7**, 10311 (2016).
81. Ziaf, K. et al. Characterization of ERD15 gene from cultivated tomato (*Solanum lycopersicum*). *Pak. J. Agric. Sci.* **53**, 27–33 (2016).
82. Aalto, M. K. et al. ERD15—an attenuator of plant ABA responses and stomatal aperture. *Plant Sci.* **182**, 19–28 (2012).
83. Kozlov, G. et al. Structural basis of ligand recognition by PABC, a highly specific peptide-binding domain found in poly(A)-binding protein and a HECT ubiquitin ligase. *EMBO J.* **23**, 272–281 (2004).
84. Kozlov, G., Menade, M., Rosenauer, A., Nguyen, L. & Gehring, K. Molecular determinants of PAM2 recognition by the MLLE domain of poly(A)-binding protein. *J. Mol. Biol.* **397**, 397–407 (2010).
85. de Torres-Zabala, M. et al. *Pseudomonas syringae* pv. tomato hijacks the *Arabidopsis* abscisic acid signalling pathway to cause disease. *EMBO J.* **26**, 1434–1443 (2007).
86. Audenaert, K., De Meyer, G. B. & Höfte, M. M. Abscisic acid determines basal susceptibility of tomato to *Botrytis cinerea* and suppresses salicylic acid-dependent signaling mechanisms. *Plant Physiol.* **128**, 491–501 (2002).
87. Amira, M. & Hegazi, A. M. E. S. Impact of salicylic acid and Paclobutrazol exogenous application on the growth, yield and nodule formation of common bean. *Aust. J. Basic Appl. Sci.* **1**, 834–840 (2007).
88. Diao, W. et al. Genome-wide analyses of the NAC transcription factor gene family in pepper (*Capsicum annuum* L.): chromosome location, phylogeny, structure, expression patterns, cis-elements in the promoter, and interaction network. *Int. J. Mol. Sci.* **19**, 1028 (2018).
89. Faria, J. A. Q. A. et al. The NAC domain-containing protein, GmNAC6, is a downstream component of the ER stress-and osmotic stress-induced NRP-mediated cell-death signaling pathway. *BMC Plant Biol.* **11**, 129 (2011).
90. Fan, G. et al. A *Phytophthora capsici* RXLR effector targets and inhibits a plant PPIase to suppress endoplasmic reticulum-mediated immunity. *Mol. Plant* **11**, 1067–1083 (2018).
91. Tyler, B. M. The fog of war: how network buffering protects plants' defense secrets from pathogens. *PLoS Genet.* **13**, e1006713 (2017).
92. Kalinina, N. O., Makarova, S., Makhotenko, A., Love, A. J. & Taliansky, M. The multiple functions of the nucleolus in plant

development, disease and stress responses. *Front. Plant Sci.* **9**, 132 (2018).
93. Lan, X. et al. *Plasmopara viticola* effector PvRXLR131 suppresses plant immunity by targeting plant receptor-like kinase inhibitor BKI1. *Mol. Plant Pathol.* **20**, 765–783 (2019).
94. Armstrong, M. R. et al. An ancestral oomycete locus contains late blight avirulence gene Avr3a, encoding a protein that is recognized in the host cytoplasm. *Proc. Natl Acad. Sci. USA* **102**, 7766–7771 (2005).
95. Jiménez-López, D., Bravo, J. & Guzmán, P. Evolutionary history exposes radical diversification among classes of interaction partners of the MLLE domain of plant poly(A)-binding proteins. *BMC Evol. Biol.* **15**, 195 (2015).
96. Petre, B. et al. Host-interactor screens of *Phytophthora infestans* RXLR proteins reveal vesicle trafficking as a major effector-targeted process. *Plant Cell* **33**, 1447–1471 (2021).
97. Rai, A. N., Tamirisa, S., Rao, K. V., Kumar, V. & Suprasanna, P. Brassica RNA binding protein ERD4 is involved in conferring salt, drought tolerance and enhancing plant growth in *Arabidopsis*. *Plant Mol. Biol.* **90**, 375–387 (2016).
98. Han, Q. et al. Salicylic acid-activated BIN2 phosphorylation of TGA3 promotes *Arabidopsis* PR gene expression and disease resistance. *EMBO J.* **4**, e110682 (2022).
99. Zhang, B. et al. Salicylic acid accelerates carbon starvation-induced leaf senescence in *Arabidopsis thaliana* by inhibiting autophagy through expressor of pathogenesis-related genes. *Plant Sci.* **336**, 111859 (2023).
100. Ton, J., Flors, V. & Mauch-Mani, B. The multifaceted role of ABA in disease resistance. *Trends Plant Sci.* **14**, 310–317 (2009).
101. Ward, E. W., Cahill, D. M. & Bhattacharyya, M. K. Abscisic acid suppression of phenylalanine ammonia-lyase activity and mRNA, and resistance of soybeans to *Phytophthora megasperma* f.sp. glycinea. *Plant Physiol.* **91**, 23–27 (1989).
102. Cao, F. Y., Yoshioka, K. & Desveaux, D. The roles of ABA in plant-pathogen interactions. *J. Plant Res.* **124**, 489–499 (2011).
103. Yu, X. et al. The RxLR effector Avh241 from *Phytophthora sojae* requires plasma membrane localization to induce plant cell death. *N. Phytol.* **196**, 247–260 (2012).
104. Wang, M., Weiberg, A., Dellota, E. Jr., Yamane, D. & Jin, H. Botrytis small RNA Bc-siR37 suppresses plant defense genes by cross-kingdom RNAi. *RNA Biol.* **14**, 421–428 (2017).
105. Xiang, J. et al. A candidate RxLR effector from *Plasmopara viticola* can elicit immune responses in *Nicotiana benthamiana*. *BMC Plant Biol.* **17**, 75 (2017).
106. Zhu, C. et al. *Phytophthora capsici* homologue of the cell cycle regulator SDA1 is required for sporangial morphology, mycelial growth and plant infection. *Mol. Plant Pathol.* **17**, 369–387 (2016).
107. Yan, H. Z. & Liou, R. F. Selection of internal control genes for real-time quantitative RT-PCR assays in the oomycete plant pathogen *Phytophthora parasitica*. *Fungal Genet. Biol.* **43**, 430–438 (2006).
108. Pfaffl, M. W. A new mathematical model for relative quantification in real-time RT-PCR. *Nucleic Acids Res.* **29**, e45 (2001).
109. Ahonsi, M. O., Banko, T. J. & Hong, C. A simple in-vitro 'wet-plate' method for mass production of *Phytophthora nicotianae* zoospores and factors influencing zoospore production. *J. Microbiol. Methods* **70**, 557–560 (2007).
110. Zhang, Y. et al. Protein kinase a regulatory subunit is required for normal growth, zoosporogenesis, and pathogenicity in *Phytophthora sojae*. *Res. Microbiol.* **11**, 104152 (2023).
111. Blanco, F. A. & Judelson, H. S. A bZIP transcription factor from *Phytophthora* interacts with a protein kinase and is required for zoospore motility and plant infection. *Mol. Microbiol.* **56**, 638–648 (2005).
112. Ma, X. et al. Identification of CBL and CIPK gene families and functional characterization of CaCIPK1 under *Phytophthora capsici* in pepper (*Capsicum annuum* L.). *BMC Genom.* **20**, 775 (2019).
113. Wang, W. et al. Sterol-sensing domain (SSD)-containing proteins in sterol auxotrophic *Phytophthora capsici* mediate sterol signaling and play a role in asexual reproduction and pathogenicity. *Microbiol Spectr.* **11**, e0379722 (2023).
114. Wan, H. et al. Identification of reference genes for reverse transcription quantitative real-time PCR normalization in pepper (*Capsicum annuum* L.). *Biochem. Biophys. Res. Commun.* **416**, 24–30 (2011).
115. Liu, D. et al. Validation of reference genes for gene expression studies in virus-infected *Nicotiana benthamiana* using quantitative real-time PCR. *PLoS One* **7**, e46451 (2012).
116. Kalderon, D., Roberts, B. L., Richardson, W. D. & Smith, A. E. A short amino acid sequence able to specify nuclear location. *Cell* **39**, 499–509 (1984).
117. Wen, W., Meinkoth, J. L., Tsien, R. Y. & Taylor, S. S. Identification of a signal for rapid export of proteins from the nucleus. *Cell* **82**, 463–473 (1995).
118. Bothwell, M. A. & Shooter, E. M. Dissociation equilibrium constant of *β* Nerve growth factor. *J. Biol. Chem.* **252**, 8532–8536 (1997).
119. Kim, H. S. et al. A NAC transcription factor and SNI1 cooperatively suppress basal pathogen resistance in *Arabidopsis thaliana*. *Nucleic Acids Res.* **40**, 9182–9192 (2012).
120. Thompson, J. D., Gibson, T. J., Plewniak, F., Jeanmougin, F. & Higgins, D. G. The CLUSTAL_X windows interface: flexible strategies for multiple sequence alignment aided by quality analysis tools. *Nucleic Acids Res.* **25**, 4876–4882 (1997).
121. Clough, S. J. & Bent, A. F. Floral dip: a simplified method for *Agrobacterium*-mediated transformation of *Arabidopsis thaliana*. *Plant J.* **16**, 735–743 (1998).
122. Valentine, T. et al. Efficient virus-induced gene silencing in roots using a modified tobacco rattle virus vector. *Plant Physiol.* **136**, 3999–4009 (2004).
123. Forcat, S., Bennett, M. H., Mansfield, J. W. & Grant, M. R. A rapid and robust method for simultaneously measuring changes in the phytohormones ABA, JA and SA in plants following biotic and abiotic stress. *Plant Methods* **4**, 16 (2008).
124. Müller, M. & Munné-Bosch, S. Rapid and sensitive hormonal profiling of complex plant samples by liquid chromatography coupled to electrospray ionization tandem mass spectrometry. *Plant Methods* **7**, 37 (2011).

Acknowledgements

This work was supported by the Special Fund for Agro-scientific Research in the Public Interest of China (grant number, CARS-25-B-03 to X.G.Z.) and the Key Research and Development Program of Shandong Province (grant number, 2019JZZY010714 to C.Y.Z.).

Author contributions

H.S., C.C.A., C.C.Y. and X.G.Z. conceived and designed the experiments. H.S., C.C.A. and C.C.Y. performed the experiments. H.S., C.C.A., C.C.Y., C.Y.Z., Z.M., F.Z.W., X.D.W., D.L.D., P.F.M. and X.G.Z. analyzed and interpreted the results. H.S., D.L.D., P.F.M. and X.G.Z. wrote this paper.

Competing interests

The authors declare no competing interests.

Additional information

Supplementary information The online version contains supplementary material available at https://doi.org/10.1038/s41467-024-50782-3.

Correspondence and requests for materials should be addressed to Xiuguo Zhang.

Peer review information *Nature Communications* thanks Franziska Trusch, Tsutomu Kawasaki and the other anonymous reviewers for their contribution to the peer review of this work. A peer review file is available.